THESIS FOR THE DEGREE OF LICENTIATE OF ENGINEERING

Theoretical quantum optics with giant atoms

ARIADNA SORO ÁLVAREZ

Department of Microtechnology and Nanoscience (MC2)
Applied Quantum Physics Laboratory
Chalmers University of Technology
Göteborg, Sweden, 2023

Theoretical quantum optics with giant atoms
ARIADNA SORO ÁLVAREZ

Technical Report MC2-461
ISSN 1652-0769

Chalmers University of Technology
Department of Microtechnology and Nanoscience (MC2)
Applied Quantum Physics Laboratory
SE–412 96 Göteborg Sweden
Telephone +46 (0)31-772 1000

Cover: Two braided giant atoms coupled to a structured waveguide, which is represented as an array of coupled cavities. The figure is part of Paper B.

Chalmers Digitaltryck
Göteborg, Sweden, 2023

Theoretical quantum optics with giant atoms
ARIADNA SORO ÁLVAREZ
Department of Microtechnology and Nanoscience (MC2)
Applied Quantum Physics Laboratory
Chalmers University of Technology

Abstract

Giant atoms have emerged as new paradigm in quantum optics during the last decade. These are quantum emitters that couple to light—or other bosonic fields—at multiple discrete points, which can be spaced wavelengths apart. In the short time since the giant-atom regime was first reached, it has been shown that they offer more possibilities for design, control, manipulation, and tunabilily than small atoms do, which makes them promising assets for quantum technologies. At the same time, due to the novelty of the field, most works to date have only studied giant atoms in relatively simple setups, e.g., coupled to open continuous waveguides. Thus, the papers appended here are an attempt to broaden the field by studying giant atoms in environments that have not been explored in depth before: continuous waveguides with chiral coupling and structured waveguides.

In this thesis, we contextualize the papers with regards to previously-existing knowledge and future applications in the fields of quantum optics and quantum technology. We also provide a detailed description of the analytical tools that are necessary to derive the results of the appended papers: we delve into Lindbladian master equations, SLH formalism, and resolvent formalism, and we focus particularly on the underlying assumptions and approximations behind these techniques.

Keywords: Quantum optics, waveguide quantum electrodynamics, open quantum systems, giant atoms, artificial atoms, continuous waveguides, structured waveguides, master equation, SLH formalism, resolvent formalism

Acknowledgments

First and foremost, I would like to express my deep gratitude to Anton Frisk Kockum, my main supervisor, for his incommensurable support, guidance, motivation and constructive criticism. Thank you for encouraging me to teach, attend courses and summer schools, present at conferences, ask for grants, and all those things that help me become a well-rounded researcher and individual. This thesis would not have been possible without you.

I would also like to offer special thanks to Carlos Sánchez Muñoz, my assistant supervisor and co-author, for always having the door open for physics discussions and reminding me how fun those can be! More special thanks go to Irina Pettersson, one of the strongest people I know, for being the best mentor and role model I could ever ask for.

I would like to express my appreciation to the present and past members of AQP for fostering such a fun working environment, packed with kickoffs, homemade fikas, sunbaths in the kitchen, afterworks at Pripps and stimulating sauna conversations. I am particularly grateful to the honorary member of AQP, Linda Brånell, whose diligence has saved me an immense amount of time in bureaucracy and has instead allowed me to spend it in research. Thank you for caring and for always having all the answers—we need more people like you!

Last but not least, I am thankful to those who partake in my other endeavors at Chalmers—the MC2 PhD student council, the DS board, Jägr, and the physics girls—, for sharing my concern that there's more to academia than research, and for helping me do something about it. You make my road to the PhD more challenging and waaaay busier, but all the more fun for it!

Ariadna Soro Álvarez, Göteborg, March 2023

Publications

A **Chiral quantum optics with giant atoms**
Ariadna Soro and Anton Frisk Kockum
Physical Review A **105**, 023712 (2022)

B **Interaction between giant atoms in a one-dimensional structured environment**
Ariadna Soro, Carlos Sánchez Muñoz, and Anton Frisk Kockum
Physical Review A **107**, 013710 (2023)

Contents

1 Introduction

What is quantum?—asked Vitaly, in a thick Russian accent and a skeptical tone, on one of my first days as a PhD student. Not the question you expect to hear from the most senior member of the Applied *Quantum* Physics division, yet I have heard him ask it many times since, to all sorts of speakers—from students to renowned researchers. *Vot is qvantum?*

To borrow from Elyse Myers, *that's a great question, I'd love to tell you.*

1.1 The quantum revolutions

At the end of the nineteenth century, scientists seemed to have understood the most fundamental principles of nature: from the motion of bodies, to the propagation of electromagnetic fields, or the laws of thermodynamics. Little did they know that the understanding of physics was about to drastically change at the turn of the century, once they started delving into the atomic and subatomic scales. Many novel counterintuitive ideas were postulated and subsequently proved: energy comes in discrete quantities known as quanta, objects have characteristics of both particle and waves, and there are limits to how accurately the value of a physical quantity can be predicted prior to its measurement. Under these principles, quantum mechanics was established, and many great inventions were created, such as the transistor, the laser, and the atomic clock. In turn, these inventions later gave us computers, optical fiber communication, and global positioning system (GPS), all of which are vital to the world as we know it today. This is what we call the *first quantum revolution* [1, 2].

Now a *second* revolution is underway—this one centered on the applicability of more complex quantum phenomena, such as superposition, entanglement, or squeezing. In this era, we not only talk about quantum mechanics or physics, but also of quantum technologies, which can be divided in four main fields according to their purpose. Quantum computing [3] aims at speeding up computation on important optimization problems; quantum simulation [4] pursues simulating complex physical systems, such as molecules for medical and chemical applications; quantum communication [5] wants to provide secure encryption and communication channels; and quantum sensing and metrology [6] aims at increasing precision and speed for a large variety of measurements.

Most of these quantum technologies have something in common: they rely on the manipulation and generation of non-classical states of light. And in order to achieve such control, it is essential to first achieve a deep understanding of quantum optical phenomena, i.e., of phenomena concerning the interactions between light and matter at the scale of individual quanta of light (photons). It was, in fact, quantum optics that kickstarted the first quantum revolution, with the modeling of the blackbody radiation spectrum by Max Planck in 1899. Since then, the field has expanded—and keeps expanding—into many directions, in part aided by emerging technologies that keep opening the door to unexplored physical paradigms.

In this thesis, we focus on a specific platform to study quantum optics: waveguide quantum electrodynamics (WQED) [7]. As the name suggests, a waveguide is a structure that guides waves with minimal energy losses by restricting the transmission of energy to one dimension. Thus, WQED is concerned with the interaction between photons propagating in a waveguide and localized quantum emitters, such as cold atoms or superconducting qubits, which are capable of emitting and absorbing single photons. More in particular, in this thesis, we use WQED to study a new paradigm of quantum emitters: the so-called *giant atoms*.

1.2 Giant atoms

In quantum optics, we have typically assumed that atoms are *small* compared to the light they interact with. That is because the radius of natural atoms ($r \approx 10^{-10}$ m) is orders of magnitude smaller than optical ($\lambda \approx 10^{-7} - 10^{-6}$ m) or microwave wavelengths ($\lambda \approx 10^{-2} - 10^{-1}$ m).

However, in the last decades, quantum optics has expanded to systems with artificial atoms, i.e., engineered quantum emitters such as quantum dots ($r \approx 10^{-9}$ m) and superconducting qubits ($r \approx 10^{-4} - 10^{-3}$ m), designed to have similar properties as natural atoms. In particular, an experiment in 2014 [8] showed that the dipole approximation is not always valid by coupling a superconducting transmon qubit [9] to surface acoustic waves [10] ($\lambda \approx 10^{-6}$ m) at multiple discrete points, spaced $\lambda/4$ apart. A subsequent theoretical study [11] coined the term *giant atom* (GA), in contrast to a *small* atom, to refer to a paradigm where a quantum emitter is large compared to the wavelength of the field it interacts with, and where the multiple coupling points lead to interference effects. A sketch illustrating the difference between a small and a giant atom is shown in Fig. 1.1.

Since 2014, several experimental demonstrations of GAs have been achieved, both with superconducting qubits coupled to surface acoustic waves [8, 13–23] and to microwave waveguides [12, 24], and many other implementations have been proposed [25, 26]. Recently, giant-atom physics have also been explored beyond the atomic paradigm (natural or artificial two-/three-level systems) into giant molecules [27–30] or giant spin ensembles [31].

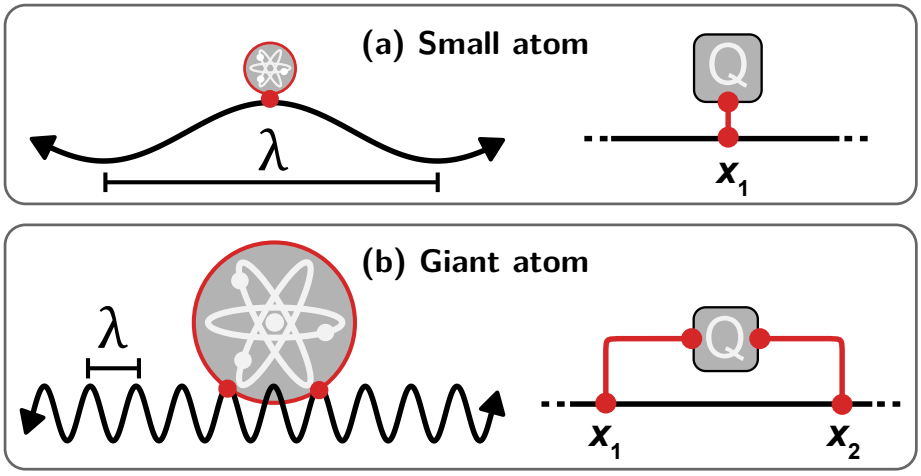

Figure 1.1: (a) A small atom, treated as a point-like object because it is much smaller than the wavelength λ of the field it interacts with. (b) A giant atom, formed by coupling a small atom to a mode at two discrete locations, spaced wavelengths apart. Figure adapted with permission from Ref. [12].

1.2.1 Properties and applications

While the appeal of GAs is partly owed to the pursuit of a fundamental understanding of light-matter interactions, the rapidly growing interest they have generated is also motivated by their potential applications in the fields of quantum computing [3] and quantum simulation [4, 32].

We present below some of the most remarkable features exhibited by GAs and how they can be harnessed.

Tunable frequency-dependent relaxation rates

In the first theory paper in GAs back in 2014, it was shown that interference between the coupling points of a GA leads to frequency-dependent relaxation rates and Lamb shifts [11]. This dependence can be engineered with a number of design parameters that increases linearly with the number of coupling points. By using superconducting qubits as GAs, the atomic frequency can be tuned in situ, making it possible to move between regions with high and low relaxation rates during an experiment, as demonstrated in Ref. [12].

If we consider more than two atomic levels, other interesting applications of the frequency-dependent relaxation rate open up. For instance, it is possible to engineer different relaxation rates for different transitions, thus allowing population inversion and lasing, which in turn, can enable electromagnetically induced transparency, as shown in Refs. [23, 24].

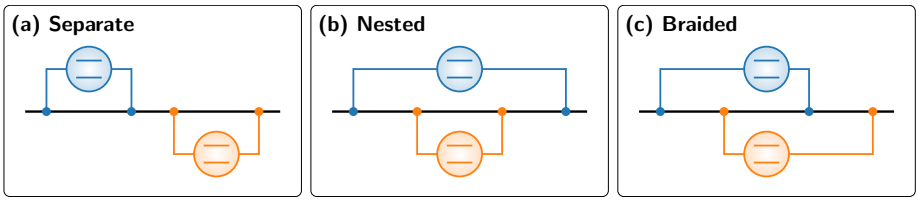

Figure 1.2: Different arrangements of two giant atoms with two coupling points each. Figure adapted from Paper B.

It is worth noting that it is also possible to engineer frequency-dependent relaxation rates and Lamb shifts by placing a small atom in front of a mirror. However, this setup is only equivalent to a GA with two coupling points in a unidirectional waveguide, and it is therefore not possible to increase the number of coupling points, to have different coupling strengths at different points, or to have more advanced scattering. This greatly limits the freedom in the design of the frequency dependence, in comparison to a giant atom. As we will explain in more detail in Chapter 3, tunable relaxation rates are also attainable for both small and giant atoms when coupling them to structured environments—but in such a case, giant atoms again offer more possibilities.

Waveguide-mediated decoherence-free interaction

Probably the most intriguing property yet found in GAs is their ability to interact though a waveguide without decohering—a feature demonstrated both theoretically [33, 34] and experimentally [12]. By arranging two or more giant atoms with their coupling points interleaved [see Fig. 1.2(c)], it is possible to suppress their individual and collective relaxation rates while maintaining their exchange interaction. In this way, they can exchange an excitation back and forth without ever losing it into the waveguide, which is something small atoms cannot do. In fact, small atoms can be prepared in so-called dark states—perfectly subradiant—that are decoupled from the waveguide. In such a case, however, only the dark state is protected from dissipation, while the decoherence-free interaction between giant atoms protects the entire atomic Hilbert space, making it much more robust and versatile. Thus, this property is of great interest in the field of quantum computing, where a major hurdle consists in preventing operation errors arising from decoherence and dissipation.

Moreover, decoherence-free interaction, together with the tunable frequency-dependent relaxation rates, helps overcoming the difficulty that small atoms pose in preparing many-body states. For instance, it has been demonstrated that GAs can be engineered to generate entangled states of the qubits to perform coherent quantum operations [12]. In the future, it may also be possible to use setups with GAs to generate cluster or graph states, which can be used for measurement-based quantum computing.

Oscillating bound states

In Ref. [35], it was shown that a giant atom with three or more coupling points can harbor oscillating bound states, i.e., dynamical exchanges of excitations between the atom and the bosonic field. In contrast to bound states arising from an impurity protected by an energy gap, the oscillating bound states appear inside the continuous energy spectrum, which makes it possible to catch and release propagating photons in the waveguide. Furthermore, since the oscillating bound states are a result of coexisting bound modes, their Hilbert space is larger than those of previously known bound states, which should enable storage and manipulation of more complex quantum states.

All in all, in the short time since the giant-atom regime was first reached, we have found that GAs offer more possibilities for design, control, manipulation, and tunabilily than small atoms do, which makes them promising assets for quantum technologies. At the same time, the field of quantum optics with giant atoms is still very new and, due to this novelty, most works to date have only studied GAs in relatively simple setups, e.g., coupled to open bidirectional continuous waveguides. The papers appended in this thesis are an attempt to broaden the field by studying GAs in environments that have not been explored in depth before: continuous waveguides with chiral coupling (Paper A) and structured waveguides (Paper B).

1.3 Outline of the thesis

This thesis is structured as follows. In Chapter 2, we present all the necessary ingredients to describe giant atoms coupled to open *continuous* waveguides—the setup studied in Paper A—, particularly in relation to the directionality of light propagation. We start with the theory of open quantum systems, including the derivation of a Lindbladian master equation and the introduction of the SLH formalism. We then transition to a more applied side of cascaded quantum systems, where we discuss chiral interfaces and ways of protecting against decoherence.

In Chapter 3, on the other hand, we delve into giant atoms coupled to *structured* waveguides, which is the setup studied in Paper B. We discuss the limitations of the tools presented in the previous chapter, and introduce the resolvent formalism and other complex-analysis techniques to overcome them. We then apply these methods to the spontaneous emission of a giant atom.

Finally, in Chapter 4, we give an overview of the appended papers, and we conclude with an outlook on future research in Chapter 5.

2 Continuous waveguides

An *open quantum system* is a quantum-mechanical system that is coupled to a surrounding *environment*, often called a *bath* or a *reservoir*. In general, this interaction changes the dynamics of the system and results in dissipation, such that the information contained in the system is lost to its environment. In quantum optical experiments, an open quantum system typically consists of one or more quantum emitters (natural or artificial atoms) coupled to an optical fiber or to a microwave transmission line (chip-integrated coaxial cable). These are types of one-dimensional (1D) *continuous waveguides*, which support a continuum of propagating modes that can be modeled by the following Hamiltonian ($\hbar = 1$ throughout this thesis):

$$H = \sum_k \omega_k \, a_k^\dagger a_k, \tag{2.1}$$

where ω_k is the frequency of each mode, and $a_k^\dagger, a_k$ are the creation and annihilation operators, respectively [7, 36–38]. Since the sum is infinite and mode spacing is infinitesimal, it is sometimes convenient to rewrite the Hamiltonian as an integral:

$$H = \int_0^\infty d\omega \, \omega \, a_\omega^\dagger a_\omega = \int_0^\infty dk \, \omega_k v_p \, a_k^\dagger a_k, \tag{2.2}$$

where v_p is the phase velocity. The dispersion relation of the bath is given by $\omega(k) = k \cdot v_p(k)$, which sets the density of states $D(\omega) = |\partial\omega(k)/\partial k|^{-1}$ [38]. Continuous waveguides usually have trivial dispersion relations, often considered linear [36, 37, 39].

In this chapter, we provide the formalism to describe the dynamics of a quantum emitter (or an ensemble of them) coupled to a 1D open waveguide, based on Refs. [40–43].

2.1 Lindbladian master equation for open quantum systems

When dealing with open quantum systems, we are interested in how the system dynamics are affected by the environment, but not so much in the dynamical

processes taking place in the environment itself. In order to provide a mathematical description of such dynamics, we derive a master equation for the system's density matrix, which includes the effects of the interaction with the bath, but traces out the bath's degrees of freedom. Since the environment consists of infinitely many quantum systems, we need to make several approximations, which fortunately are well justified in most experiments.

To illustrate the derivation of a master equation, we consider a model where our quantum system is a two-level atom, coupled to a bath of an infinite number of harmonic oscillators. The total Hamiltonian H is then the sum of the atomic Hamiltonian H_a, the bath Hamiltonian H_b, and their interaction H_{int}:

$$H = H_a + H_b + H_{\text{int}}, \tag{2.3}$$

$$H_a = \frac{\omega_a}{2}\sigma_z, \tag{2.4}$$

$$H_b = \sum_k \omega_k \, a_k^\dagger a_k, \tag{2.5}$$

$$H_{\text{int}} = \sum_k g_k (a_k + a_k^\dagger)(\sigma_- + \sigma_+), \tag{2.6}$$

where ω_a is the transition frequency of the atom; σ_z is the Pauli-Z matrix; $\sigma_\pm$ are the ladder operators of the atom, such that $\sigma_+\sigma_- = (1 + \sigma_z)/2$; and g_k denotes the coupling strength between the atom and the bath.

Let $\rho_{\text{tot}}(t)$ be the density operator of the total system (atom plus bath). Then the Schrödinger equation reads

$$\dot{\rho}_{\text{tot}} = -i[H, \rho_{\text{tot}}], \tag{2.7}$$

with H given by Eq. (2.3). In the interaction picture, henceforth denoted by $\sim$, we can write Eq. (2.7) by separating the rapid motion generated by $H_a + H_b$ from the slow motion generated by H_{int}. Defining

$$\tilde{\rho}_{\text{tot}}(t) \equiv e^{i(H_a+H_b)t} \rho_{\text{tot}}(t) e^{-i(H_a+H_b)t}, \tag{2.8}$$

we obtain

$$\dot{\tilde{\rho}}_{\text{tot}}(t) = -i[\tilde{H}_{\text{int}}(t), \tilde{\rho}_{\text{tot}}(t)], \tag{2.9}$$

the solution of which is

$$\tilde{\rho}_{\text{tot}}(t) = \tilde{\rho}_{\text{tot}}(0) - i \int_0^t d\tau \Big[\tilde{H}_{\text{int}}(\tau), \tilde{\rho}_{\text{tot}}(\tau)\Big]. \tag{2.10}$$

By inserting Eq. (2.10) into Eq. (2.9) and tracing over the the bath degrees of freedom, we obtain an equation for the atomic density matrix ρ_a:

$$\dot{\tilde{\rho}}_a(t) = \text{Tr}_b \left\{ -i\Big[\tilde{H}_{\text{int}}(t), \tilde{\rho}_{\text{tot}}(0)\Big] - \int_0^t d\tau \Big[\tilde{H}_{\text{int}}(t), \Big[\tilde{H}_{\text{int}}(\tau), \tilde{\rho}_{\text{tot}}(\tau)\Big]\Big] \right\}. \tag{2.11}$$

Note that all steps from Eq. (2.7) to Eq. (2.11) are exact and generalizeable to any Hamiltonian of the form Eq. (2.3). To go forward, however, we need to make some approximations.

2.1.1 Born, Markov, and rotating-wave approximations

The *Born approximation* is based on the coupling g_k being weak and the reservoir being large enough to be virtually unaffected by its interaction with the atom. In this approximation, we first assume that the interaction is turned on at $t = 0$ and that no correlations exist between the system and the bath at this initial time. Therefore, the initial state factorizes as $\rho_{\text{tot}}(0) = \rho_a(0) \otimes \rho_b(0)$. At later times, correlations between the system and the bath arise due to their coupling. However, since we assume that the coupling is very weak and $\rho_{\text{tot}}(t)$ should only show deviations of order H_{int} from an uncorrelated state, we can neglect higher-order terms, i.e., $\tilde{\rho}_{\text{tot}}(t) = \tilde{\rho}_a(t)\rho_b(0) + O(H_{\text{int}})$. Then, Eq. (2.11) becomes, under the Born approximation,

$$\dot{\tilde{\rho}}_a(t) = -\int_0^t d\tau \, \text{Tr}_b \left\{ \left[\tilde{H}_{\text{int}}(t), \left[\tilde{H}_{\text{int}}(\tau), \tilde{\rho}_a(\tau)\rho_b(0) \right] \right] \right\}. \tag{2.12}$$

The *Markov approximation* states that the bath has no memory, i.e., that any imprint the atom makes on the bath at time t_1 does not affect the dynamics at a later time t_2. It can be understood as follows: if the reservoir is large, we do not expect it to preserve the minor changes caused by its interaction with the atom for very long—at least, not long enough to significantly affect the future evolution of the atom. Therefore, we can replace $\tilde{\rho}_a(\tau)$ in Eq. (2.12) with $\tilde{\rho}_a(t)$ to obtain a master equation in the *Born-Markov approximation*:

$$\dot{\tilde{\rho}}_a(t) = -\int_0^t d\tau \, \text{Tr}_b \left\{ \left[\tilde{H}_{\text{int}}(t), \left[\tilde{H}_{\text{int}}(\tau), \tilde{\rho}_a(t)\rho_b(0) \right] \right] \right\}. \tag{2.13}$$

To proceed from here is quite straightforward, so the remaining details of the derivation are left out of the scope of this thesis and we refer the interested reader to Refs. [40, 44].

The only non-trivial step left to take is the *rotating-wave approximation* (RWA), through which we neglect the fast oscillating terms [45]. Explicitly, the RWA is applied in the interaction picture, where terms in the Hamiltonians that oscillate with frequencies $\omega_a + \omega_b$ are neglected, while terms that oscillate with frequencies $\omega_a - \omega_b$ are kept. This is a valid approximation when the bath frequency ω_b is close to the atomic transition ω_a, and the coupling is weak (i.e., when $\omega_a, \omega_b \gg g$), which is a safe assumption to make in the optical and microwave regimes.

Finally, after all approximations have been made and the bath has been traced out, we can transform back from the interaction picture to obtain a master equation in the *Lindblad* form:

$$\dot{\rho}_a = -i\left[\frac{\omega_a'}{2}\sigma_z, \rho_a \right] + \Gamma \mathcal{D}[\sigma_-]\rho_a, \tag{2.14}$$

where $\mathcal{D}[X]\rho = X\rho X^\dagger - \frac{1}{2}\{X^\dagger X, \rho\}$ are Lindblad superoperators, Γ is the atomic relaxation rate, and ω_a' is the Lamb-shifted transition frequency. In a

small atom, the relaxation rate is given by

$$\Gamma_{\text{small}} = 2\pi D(\omega_a) g^2(\omega_a), \tag{2.15}$$

where $D(\omega)$ is the bath density of states and $g(\omega_k) = g_k$ is the coupling strength [11]. For a giant atom, Γ also accounts for the interference between coupling points and it therefore depends on the spacing between the points. As we will see in subsequent examples [see, e.g., Table 2.1], it can take values up to $\Gamma_{\text{giant}} \leq N^2 \Gamma_{\text{small}}$, where N is the number of coupling points [44].

It should be noted that we could have made the RWA earlier, for instance, directly on H_{int} in Eq. (2.6), by neglecting the terms $a\sigma_-$ and $a^\dagger \sigma^+$. However, while that is a very common practice, it carries the consequence that ω_a' does not accurately capture the Lamb shift of the transition frequency [40, 46, 47]. Thus, only if we are not interested in the exact value of the frequency shift we can apply the RWA directly on the Hamiltonian, which is the case in both appended papers.

A master-equation treatment like the one presented in this section is used in Paper A to study the waveguide-mediated interaction between giant atoms in a chiral setting. While such an approach had been used before for giant atoms [33], variations in the direction of propagation of light had not been considered. Since the setup in Paper A deals with more interconnected systems and a more complex system-bath interaction, an accurate description of it requires some additional formalism beyond the master equation derived here. In particular, we use the SLH formalism, which we introduce in the following section.

2.2 SLH framework for quantum networks

The SLH framework [41–43] was developed in 2009 to model *quantum input-output networks*, i.e., quantum optical networks made of local components that interact via itinerant quantum bosonic fields. Its conception was motivated by the need to simplify complicated descriptions of networks containing *cascaded quantum systems* [48, 49], where the output from one system is used as the input for another.

The SLH formalism is a modular framework where each local component is treated as a black box that scatters the propagating fields according to some pre-specified input-output behavior. In addition, it incorporates the quantum nature of the itinerant fields and any quantum dynamics in the localized components. The power of the SLH formalism lies in its ability to compose the propagator for local components according to how they are connected in a network.

In this section, we show the basics of the formalism and how it can be used in conjunction with the master equation—a combination that we used to model the setup in Paper A.

2.2.1 SLH formalism

In the SLH formalism, an open quantum system with n input-output ports is described by a triplet $G = (\mathcal{S}, \mathcal{L}, H)$, where $\mathcal{S}$ is an $n \times n$ scattering matrix, $\mathcal{L}$ is an $n \times 1$ vector representing the coupling between the system and the environment at the input-output ports, and H is the Hamiltonian of the system. Let us elucidate why.

Consider two cascaded quantum systems with Hamiltonians H_1 and H_2, such that the output from system 1 becomes the input to system 2. Both systems are coupled via an input-output port to the environment, by coupling operators $\mathcal{L}_1$ and $\mathcal{L}_2$, respectively. Through input-output theory and quantum stochastic calculus, it can be shown that the total system behaves as if it had a Hamiltonian $H = H_1 + H_2 + (\mathcal{L}_2^\dagger \mathcal{L}_1 - \mathcal{L}_1^\dagger \mathcal{L}_2)/(2i)$ and was coupled to the environment via an operator $\mathcal{L} = \mathcal{L}_1 + \mathcal{L}_2$ [43, 44, 50]. This suggests that an open quantum system could be assigned a doublet $G = (\mathcal{L}, H)$, and that the doublet corresponding to two quantum systems *in series* would defined as follows:

$$G = G_2 \triangleleft G_1 = (\mathcal{L}_2, H_2) \triangleleft (\mathcal{L}_1, H_1) = \left(\mathcal{L}_1 + \mathcal{L}_2, H_1 + H_2 + \frac{1}{2i}(\mathcal{L}_2^\dagger \mathcal{L}_1 - \mathcal{L}_1^\dagger \mathcal{L}_2) \right) \tag{2.16}$$

Now, the doublet above is still missing the $\mathcal{S}$ in SLH, i.e., the scattering matrix. For a single-channel case, the $\mathcal{S}$ may describe the non-negligible distance between two systems G_1 and G_2 through, for instance, an acquired phase shift ϕ, which is inserted by placing the triplet $G_\phi = (e^{i\phi}, 0, 0)$ between G_1 and G_2. Note that in such a case, the time it takes for an excitation to travel between systems must be small compared to the timescale of the systems' evolution.

On the other hand, the scattering matrix is also essential to describe many-channel systems such as beamsplitters or circulators, which take several inputs and mix them into several outputs.

Finally, another widely used component is the coherent drive. For example, a coherent signal of $|\beta|^2$ photons per second can be represented by the triplet $G_\beta = (1, \beta, 0)$.

2.2.2 SLH composition rules

Now that we have introduced the different components of the SLH triplet, we can compose them to build more complex quantum networks. For that, we need the three fundamental composition rules for the SLH formalism: the series product, the concatenation product, and the feedback operation (see Fig. 2.1).

As shown in Eq. (2.16), the *series product* is denoted by $\triangleleft$ and describes systems which are laid out in a cascaded way. Now accounting for the scattering matrix, the series product is defined as:

$$G_2 \triangleleft G_1 = \left(\mathcal{S}_2 \mathcal{S}_1, \;\; \mathcal{S}_2 \mathcal{L}_1 + \mathcal{L}_2, H_1 + H_2 + \frac{1}{2i} \left(\mathcal{L}_2^\dagger \mathcal{S}_2 \mathcal{L}_1 - \mathcal{L}_1^\dagger \mathcal{S}_2^\dagger \mathcal{L}_2 \right) \right), \tag{2.17}$$

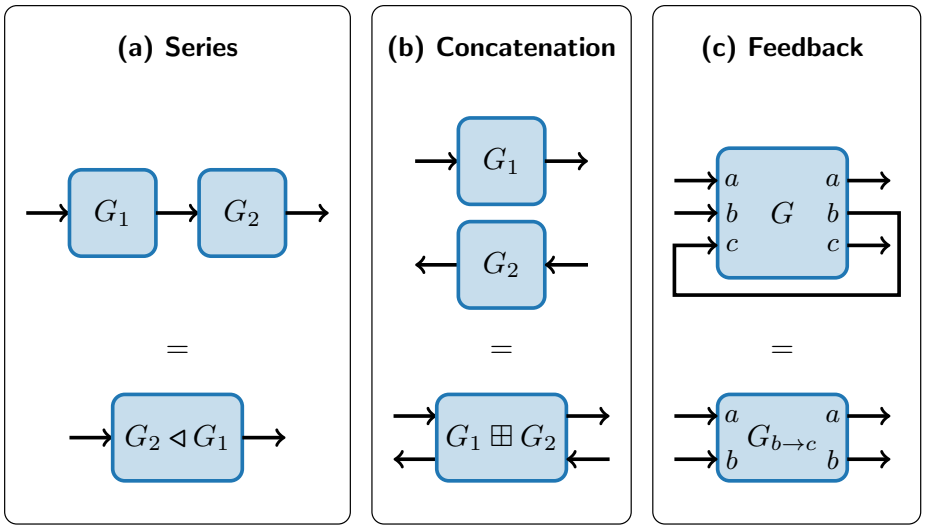

Figure 2.1: The three SLH composition rules: (a) series product, (b) concatenation product, (c) feedback operation.

which we note does not commute, i.e., it is not invariant under the permutation of 1 and 2.

The *concatenation product* is denoted by $\boxplus$ and is used in processes that occur in parallel, and there is therefore no need to let one system evolve before calculating the evolution of the other. Mathematically, it is defined as:

$$G_1 \boxplus G_2 = \left(\begin{pmatrix} \mathcal{S}_1 & 0 \\ 0 & \mathcal{S}_2 \end{pmatrix}, \begin{pmatrix} \mathcal{L}_1 \\ \mathcal{L}_2 \end{pmatrix}, H_1 + H_2 \right). \tag{2.18}$$

The concatenation product may also be generalized to consider the case where G_1 is directly coupled to G_2 by some interaction H_{int}. Then, we would just need to replace H_1 by $H_1 + H_{\text{int}}$ in Eq. (2.18).

The *feedback* operation describes the process of feeding the x-th output of a system into the y-th input of the same system, a link denoted by $x \to y$. As shown in Fig. 2.1(c), this interconnection results in a triplet of reduced dimension $G_{x\to y} = (\mathcal{S}_{\text{red}}, \mathcal{L}_{\text{red}}, H_{\text{red}})$, where

$$\begin{aligned} \mathcal{S}_{\text{red}} &= \mathcal{S}_{\cancel{x},\cancel{y}} + \mathcal{S}_{\cancel{x},y}(1 - \mathcal{S}_{x,y})^{-1}\mathcal{S}_{x,\cancel{y}} \\ \mathcal{L}_{\text{red}} &= \mathcal{L}_{\cancel{x}} + \mathcal{S}_{\cancel{x},y}(1 - \mathcal{S}_{x,y})^{-1}\mathcal{L}_x \\ H_{\text{red}} &= H + \frac{1}{2i}\left(\mathcal{L}^\dagger \mathcal{S}_{:,y}(1 - \mathcal{S}_{x,y})^{-1}\mathcal{L}_x - \text{H.c.}\right), \end{aligned} \tag{2.19}$$

and $\mathcal{S}_{\cancel{x},\cancel{y}}$ is the scattering matrix with row x and column y removed; $\mathcal{S}_{\cancel{x},y}$ ($\mathcal{S}_{x,\cancel{y}}$) denotes the column y (row x) of the matrix with the x-th (y-th) element removed; $\mathcal{S}_{:,y}$ is the entire y-th column; $\mathcal{S}_{x,y}$ denotes the element xy; $\mathcal{L}_{\cancel{x}}$ refers to

the coupling vector with the x-th element removed; $\mathcal{L}_x$ is the x-th element of the vector; and H.c. denotes Hermitian conjugate.

These three composition rules are sufficient to describe any arbitrary quantum network that satisfies (i) the Born-Markov approximation, (ii) that the bosonic fields propagate in a linear medium without dispersion, and (iii) that the travel time between components is negligible compared to the relaxation times of the systems. In fact, once we calculate the triplet $G = (\mathcal{S}, \mathcal{L}, H)$ of the network, we can extract the master equation

$$\dot{\rho} = -i[H, \rho] + \sum_{j=1}^{n} \mathcal{D}[\mathcal{L}_j]\rho. \tag{2.20}$$

2.2.3 Example: two atoms chirally coupled to a continuous waveguide

Let us illustrate the SLH formalism for two small atoms [Fig. 2.2(a)] and two giant braided atoms [Fig. 2.2(b)], which are some of the elementary setups studied in Paper A.

Let us consider two atoms A and B with resonant frequencies ω_A and ω_B, respectively[1]. Taking the atoms to be two-level systems, their Hamiltonians can be written as

$$H_A = \frac{\omega_A}{2}\sigma_z^A, \quad H_B = \frac{\omega_B}{2}\sigma_z^B, \tag{2.21}$$

regardless of whether they are small or giant.

The atoms are coupled to the waveguide at connection points identified by their position x_k and their bare relaxation rates γ_k, for $k = 1, 2, 3, 4$. At each coupling point, we distinguish the decay rate to the right- and left-propagating modes as γ_{kR} and γ_{kL}, in such a way that $\gamma_{kR} + \gamma_{kL} = \gamma_k$. The phase shifts acquired between neighbouring coupling points are denoted by $\phi_k = \omega|x_{k+1} - x_k|/v$ for $k = 1, 2, 3$, where ω and v are the frequency and velocity of the traveling bosons, respectively. Note that in order for the setup to be consistent with the assumptions behind the SLH formalism, we need to assume that the coupling of each atom is weak compared to their transition frequency, and that the travel time between connection points is negligible compared to the relaxation times of all the atoms. Finally, in each propagation direction, we can model the coupling between an atom j and the waveguide at a connection point k with the jump operator $\mathcal{L}$, in such a way that $\mathcal{L}_k = \sqrt{\gamma_k}\sigma_-^j$.

With all the elements we established, we can now define an SLH triplet at each connection point k:

$$G_k = \begin{cases} \left(1,\ \sqrt{\gamma_k}\sigma_-^j,\ \frac{1}{2}\omega_j\sigma_z^j\right) & \text{if } k \text{ is the first coupling point of atom } j \\ \left(1,\ \sqrt{\gamma_k}\sigma_-^j,\ 0\right) & \text{otherwise.} \end{cases} \tag{2.22}$$

[1]Not to be confused with the subscripts a, b from Sec. 2.1 denoting atom and bath.

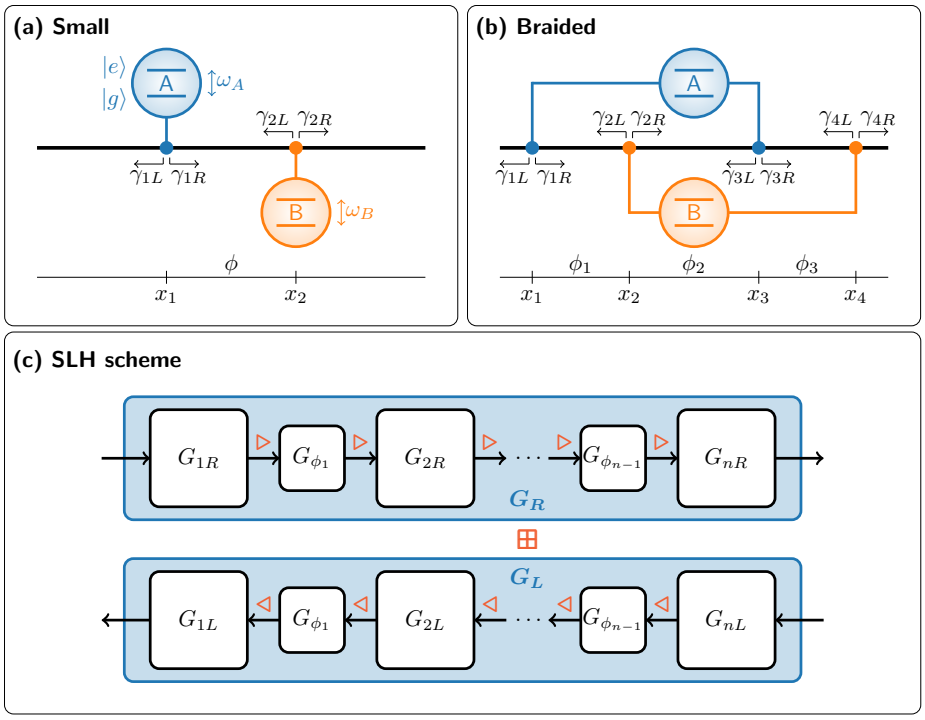

Figure 2.2: Atoms coupled to a 1D continuous open waveguide. (a, b) A sketch for (a) two small atoms, and (b) two giant braided atoms showing the relevant parameters. (c) The SLH scheme that describes the input-output flows from the setups in (a) and (b), and which is also applicable to an arbitrary number of atoms with an arbitrary number of coupling points. All figures are adapted from Paper A.

To account for the phase shift acquired between connection points k and $k+1$, we define

$$G_{\phi_k} = (e^{i\phi_k}, 0, 0). \tag{2.23}$$

We then take each propagation direction (right and left) separately and apply a series product between all the triplets, as if the system was cascaded

[see Eq. (2.17)]. In particular, for two *small* atoms, that is

$$\begin{aligned}
G_R\Big|_{\text{sma}} &= G_{2R} \lhd G_\phi \lhd G_{1R} = \\
&= \left(1,\, \sqrt{\gamma_{2R}}\,\sigma_-^B,\, \frac{1}{2}\omega_B\sigma_z^B\right) \lhd (e^{i\phi},\, 0,\, 0) \lhd \left(1,\, \sqrt{\gamma_{1R}}\,\sigma_-^A,\, \frac{1}{2}\omega_A\sigma_z^A\right) = \\
&= \Bigg(e^{i\phi},\; e^{i\phi}\sqrt{\gamma_{1R}}\,\sigma_-^A + \sqrt{\gamma_{2R}}\,\sigma_-^B, \\
&\qquad \frac{\omega_A}{2}\sigma_z^A + \frac{\omega_B}{2}\sigma_z^B + \frac{\sqrt{\gamma_{1R}\gamma_{2R}}}{2i}[e^{i\phi}\sigma_-^A\sigma_+^B - \text{H.c.}] \Bigg),
\end{aligned} \tag{2.24}$$

$$\begin{aligned}
G_L\Big|_{\text{sma}} &= G_{1L} \lhd G_\phi \lhd G_{2L} = \\
&= \left(1,\, \sqrt{\gamma_{1L}}\,\sigma_-^A,\, \frac{1}{2}\omega_A\sigma_z^A\right) \lhd (e^{i\phi},\, 0,\, 0) \lhd \left(1,\, \sqrt{\gamma_{2L}}\,\sigma_-^B,\, \frac{1}{2}\omega_B\sigma_z^B\right) = \\
&= \Bigg(e^{i\phi},\; \sqrt{\gamma_{1L}}\,\sigma_-^A + e^{i\phi}\sqrt{\gamma_{2L}}\,\sigma_-^B, \\
&\qquad \frac{\omega_A}{2}\sigma_z^A + \frac{\omega_B}{2}\sigma_z^B + \frac{\sqrt{\gamma_{1L}\gamma_{2L}}}{2i}[e^{i\phi}\sigma_-^B\sigma_+^A - \text{H.c.}] \Bigg).
\end{aligned} \tag{2.25}$$

Similarly, for two *giant braided* atoms, the triplets are

$$\begin{aligned}
G_R\Big|_{\text{bra}} &= G_{4R} \lhd G_{\phi_3} \lhd G_{3R} \lhd G_{\phi_2} \lhd G_{2R} \lhd G_{\phi_1} \lhd G_{1R} = \\
&= \left(1,\, \sqrt{\gamma_{4R}}\,\sigma_-^B,\, 0\right) \lhd (e^{i\phi_3},\, 0,\, 0) \lhd \left(1,\, \sqrt{\gamma_{3R}}\,\sigma_-^B,\, 0\right) \lhd (e^{i\phi_2},\, 0,\, 0) \\
&\quad \lhd \left(1,\, \sqrt{\gamma_{2R}}\,\sigma_-^B,\, \frac{\omega_B}{2}\sigma_z^B\right) \lhd (e^{i\phi_1},\, 0,\, 0) \lhd \left(1,\, \sqrt{\gamma_{1R}}\,\sigma_-^B,\, \frac{\omega_A}{2}\sigma_z^A\right),
\end{aligned} \tag{2.26}$$

which results in the components

$$\begin{aligned}
\mathcal{S}_R\Big|_{\text{bra}} &= e^{i(\phi_1+\phi_2+\phi_3)}, \\
\mathcal{L}_R\Big|_{\text{bra}} &= \left(e^{i(\phi_1+\phi_2+\phi_3)}\sqrt{\gamma_{1R}} + e^{i\phi_3}\sqrt{\gamma_{3R}}\right)\sigma_-^A + \left(e^{i(\phi_2+\phi_3)}\sqrt{\gamma_{2R}} + \sqrt{\gamma_{4R}}\right)\sigma_-^B, \\
H_R\Big|_{\text{bra}} &= \frac{1}{2}(\omega_A + \sin(\phi_1+\phi_2)\sqrt{\gamma_{1R}\gamma_{3R}})\sigma_z^A \\
&\quad + \frac{1}{2}(\omega_B + \sin(\phi_2+\phi_3)\sqrt{\gamma_{2R}\gamma_{4R}})\sigma_z^B \\
&\quad + \frac{1}{2i}\Big[\Big(e^{i\phi_1}\sqrt{\gamma_{1R}\gamma_{2R}} + e^{i(\phi_1+\phi_2+\phi_3)}\sqrt{\gamma_{1R}\gamma_{4R}} - e^{-i\phi_2}\sqrt{\gamma_{2R}\gamma_{3R}} \\
&\qquad + e^{i\phi_3}\sqrt{\gamma_{3R}\gamma_{4R}}\Big)\sigma_-^A\sigma_+^B - \text{H.c.}\Big],
\end{aligned} \tag{2.27}$$

and

$$\begin{aligned} G_L\Big|_{\text{bra}} &= G_{1L} \triangleleft G_{\phi_1} \triangleleft G_{2L} \triangleleft G_{\phi_2} \triangleleft G_{3L} \triangleleft G_{\phi_3} \triangleleft G_{4L} = \\ &= \Big(1,\, \sqrt{\gamma_{1L}}\,\sigma_-^B,\, \frac{\omega_A}{2}\sigma_z^A\Big) \triangleleft (e^{i\phi_1},\, 0,\, 0) \triangleleft \Big(1,\, \sqrt{\gamma_{2L}}\,\sigma_-^B,\, \frac{\omega_B}{2}\sigma_z^B\Big) \\ &\quad \triangleleft (e^{i\phi_2},\, 0,\, 0) \triangleleft \big(1,\, \sqrt{\gamma_{3L}}\,\sigma_-^B,\, 0\big) \triangleleft (e^{i\phi_3},\, 0,\, 0) \triangleleft \big(1,\, \sqrt{\gamma_{4L}}\,\sigma_-^B,\, 0\big)\,, \end{aligned} \tag{2.28}$$

which results in the components

$$\begin{aligned} \mathcal{S}_L\Big|_{\text{bra}} =& e^{i(\phi_1+\phi_2+\phi_3)}, \\ \mathcal{L}_L\Big|_{\text{bra}} =& \Big(\sqrt{\gamma_{1L}} + e^{i(\phi_1+\phi_2)}\sqrt{\gamma_{3L}}\Big)\,\sigma_-^A + \Big(e^{i\phi_1}\sqrt{\gamma_{2L}} + e^{i(\phi_1+\phi_2+\phi_3)}\sqrt{\gamma_{4L}}\Big)\,\sigma_-^B, \\ H_L\Big|_{\text{bra}} =& \frac{1}{2}(\omega_A + \sin(\phi_1+\phi_2)\sqrt{\gamma_{1L}\gamma_{3L}})\sigma_z^A \\ &+ \frac{1}{2}(\omega_B + \sin(\phi_2+\phi_3)\sqrt{\gamma_{2L}\gamma_{4L}})\sigma_z^B \\ &+ \frac{1}{2i}\Big[\Big(-e^{-i\phi_1}\sqrt{\gamma_{1L}\gamma_{2L}} - e^{-i(\phi_1+\phi_2+\phi_3)}\sqrt{\gamma_{1L}\gamma_{4L}} \\ &\quad + e^{i\phi_2}\sqrt{\gamma_{2L}\gamma_{3L}} - e^{-i\phi_3}\sqrt{\gamma_{3L}\gamma_{4L}}\Big)\sigma_-^A\sigma_+^B - \text{H.c.}\Big]. \end{aligned} \tag{2.29}$$

Now, since propagation to the right and left directions occurs simultaneously, we can concatenate the two triplets G_R and G_L according to SLH practice, such that $G = G_R \boxplus G_L$ [see Eq. (2.18)]. This yields the components

$$\begin{aligned} \mathcal{S}\Big|_{\text{sma}} &= \begin{pmatrix} e^{i\phi} & 0 \\ 0 & e^{i\phi} \end{pmatrix} \\ \mathcal{L}\Big|_{\text{sma}} &= \begin{pmatrix} e^{i\phi}\sqrt{\gamma_{1R}}\,\sigma_-^A + \sqrt{\gamma_{2R}}\,\sigma_-^B \\ \sqrt{\gamma_{1L}}\,\sigma_-^A + e^{i\phi}\sqrt{\gamma_{2L}}\,\sigma_+^B \end{pmatrix} \\ H\Big|_{\text{sma}} &= \frac{\omega_A}{2}\sigma_z^A + \frac{\omega_B}{2}\sigma_z^B + \frac{1}{2i}\Big[\Big(e^{i\phi}\sqrt{\gamma_{1R}\gamma_{2R}} - e^{-i\phi}\sqrt{\gamma_{1L}\gamma_{2L}}\Big)\sigma_-^A\sigma_+^B - \text{H.c.}\Big], \end{aligned} \tag{2.30}$$

and

$$
\begin{aligned}
\mathcal{S}\Big|_{\text{bra}} =& \begin{pmatrix} e^{i(\phi_1+\phi_2+\phi_3)} & 0 \\ 0 & e^{i(\phi_1+\phi_2+\phi_3)} \end{pmatrix} \\
\mathcal{L}\Big|_{\text{bra}} =& \begin{pmatrix} \left(e^{i(\phi_1+\phi_2+\phi_3)}\sqrt{\gamma_{1R}} + e^{i\phi_3}\sqrt{\gamma_{3R}}\right)\sigma_-^A + \left(e^{i(\phi_2+\phi_3)}\sqrt{\gamma_{2R}} + \sqrt{\gamma_{4R}}\right)\sigma_-^B \\ \left(\sqrt{\gamma_{1L}} + e^{i(\phi_1+\phi_2)}\sqrt{\gamma_{3L}}\right)\sigma_-^A + \left(e^{i\phi_1}\sqrt{\gamma_{2L}} + e^{i(\phi_1+\phi_2+\phi_3)}\sqrt{\gamma_{4L}}\right)\sigma_-^B \end{pmatrix} \\
H\Big|_{\text{bra}} =& \frac{1}{2}(\omega_A + \sin(\phi_1+\phi_2)(\sqrt{\gamma_{1R}\gamma_{3R}} + \sqrt{\gamma_{1L}\gamma_{3L}}))\sigma_z^A \\
&+ \frac{1}{2}(\omega_B + \sin(\phi_2+\phi_3)(\sqrt{\gamma_{2R}\gamma_{4R}} + \sqrt{\gamma_{2L}\gamma_{4L}}))\sigma_z^B \\
&+ \frac{1}{2i}\Big[\Big(e^{i\phi_1}\sqrt{\gamma_{1R}\gamma_{2R}} + e^{i(\phi_1+\phi_2+\phi_3)}\sqrt{\gamma_{1R}\gamma_{4R}} - e^{-i\phi_2}\sqrt{\gamma_{2R}\gamma_{3R}} \\
&\quad + e^{i\phi_3}\sqrt{\gamma_{3R}\gamma_{4R}} - e^{-i\phi_1}\sqrt{\gamma_{1L}\gamma_{2L}} - e^{-i(\phi_1+\phi_2+\phi_3)}\sqrt{\gamma_{1L}\gamma_{4L}} \\
&\quad + e^{i\phi_2}\sqrt{\gamma_{2L}\gamma_{3L}} - e^{-i\phi_3}\sqrt{\gamma_{3L}\gamma_{4L}}\Big)\sigma_-^A\sigma_+^B - \text{H.c.}\Big],
\end{aligned}
\tag{2.31}
$$

for small and braided atoms, respectively.

Finally, with the triplets above, we can compute the time evolution of the density matrix according to the master equation in Eq. (2.20), which results in an expression of the form

$$
\begin{aligned}
\dot{\rho} =& -i[H,\rho] + \sum_{j=1}^{n}\mathcal{D}[\mathcal{L}_j]\rho = \\
=& -i\left[\omega_A'\frac{\sigma_z^A}{2} + \omega_B'\frac{\sigma_z^B}{2} + \left(g\sigma_-^A\sigma_+^B + \text{H.c.}\right), \rho\right] \\
&+ \Gamma_A\mathcal{D}[\sigma_-^A]\rho + \Gamma_B\mathcal{D}[\sigma_-^B]\rho \\
&+ \left[\Gamma_{\text{coll}}\left(\sigma_-^A\rho\sigma_+^B - \frac{1}{2}\left\{\sigma_-^A\sigma_+^B, \rho\right\}\right) + \text{H.c.}\right],
\end{aligned}
\tag{2.32}
$$

where $\omega_j' = \omega_j + \delta\omega_j$ is the Lamb-shifted frequency of atom $j \in \{A, B\}$, g is the *exchange interaction* between atoms, Γ_j is the *individual relaxation rate* of atom j, and Γ_{coll} is the *collective relaxation rate* for the atoms. The exact expressions for these parameters are shown in Table 2.1.

On the one hand, the exchange interaction g is set by emission from connection points of one atom being absorbed at connection points of the other atom, and it is the complex term in the Hamiltonians from Eqs. (2.30)–(2.31).

On the other hand, the relaxation rates $\Gamma_j, \Gamma_{\text{coll}}$ are set by interference between emission from connection points belonging to the same atom (Γ_j), and different atoms (Γ_{coll}). They relate to the right (R) and left (L) collapse operators from Eqs. (2.30)–(2.31) as follows:

$$
\mathcal{L}_{R/L} = \sqrt{\Gamma_{A,R/L}}\,\sigma_-^A + \sqrt{\Gamma_{B,R/L}}\,\sigma_-^B,
\tag{2.33}
$$

Table 2.1: Frequency shifts, exchange interaction, individual and collective decays [$\delta\omega_j, g, \Gamma_j, \Gamma_{\rm coll}$ in Eq. (2.32)] for small and braided giant atoms chirally coupled to a 1D open waveguide. We assume arbitrary phase shifts ϕ_1, ϕ_2, ϕ_3 and arbitrary bare relaxation rates γ_{kR}, γ_{kL} at each coupling point $k = 1, 2, 3, 4$.

Parameter	Topology	Expression for two atoms, A and B
Frequency shifts, $\delta\omega_A$, $\delta\omega_B$	Small	0 0
	Braided	$\sin(\phi_1+\phi_2)(\sqrt{\gamma_{1R}\gamma_{3R}}+\sqrt{\gamma_{1L}\gamma_{3L}})$ $\sin(\phi_2+\phi_3)(\sqrt{\gamma_{2R}\gamma_{4R}}+\sqrt{\gamma_{2L}\gamma_{4L}})$
Individual decays, Γ_A, Γ_B	Small	$\gamma_{1R}+\gamma_{1L}$ $\gamma_{2R}+\gamma_{2L}$
	Braided	$\gamma_{1R}+\gamma_{1L}+\gamma_{3R}+\gamma_{3L}$ $+2\cos(\phi_1+\phi_2)(\sqrt{\gamma_{1R}\gamma_{3R}}+\sqrt{\gamma_{1L}\gamma_{3L}})$ $\gamma_{2R}+\gamma_{2L}+\gamma_{4R}+\gamma_{4L}$ $+2\cos(\phi_2+\phi_3)(\sqrt{\gamma_{2R}\gamma_{4R}}+\sqrt{\gamma_{2L}\gamma_{4L}})$
Collective decay, $\Gamma_{\rm coll}$	Small	$e^{i\phi}\sqrt{\gamma_{1R}\gamma_{2R}}+e^{-i\phi}\sqrt{\gamma_{1L}\gamma_{2L}}$
	Braided	$e^{i\phi_1}\sqrt{\gamma_{1R}\gamma_{2R}}+e^{i(\phi_1+\phi_2+\phi_3)}\sqrt{\gamma_{1R}\gamma_{4R}}$ $+e^{-i\phi_2}\sqrt{\gamma_{2R}\gamma_{3R}}+e^{i\phi_3}\sqrt{\gamma_{3R}\gamma_{4R}}$ $+e^{-i\phi_1}\sqrt{\gamma_{1L}\gamma_{2L}}+e^{-i(\phi_1+\phi_2+\phi_3)}\sqrt{\gamma_{1L}\gamma_{4L}}$ $+e^{i\phi_2}\sqrt{\gamma_{2L}\gamma_{3L}}+e^{-i\phi_3}\sqrt{\gamma_{3L}\gamma_{4L}}$
Exchange interaction, g	Small	$[e^{i\phi}\sqrt{\gamma_{1R}\gamma_{2R}}-e^{-i\phi}\sqrt{\gamma_{1L}\gamma_{2L}}]/2i$
	Braided	$[e^{i\phi_1}\sqrt{\gamma_{1R}\gamma_{2R}}+e^{i(\phi_1+\phi_2+\phi_3)}\sqrt{\gamma_{1R}\gamma_{4R}}$ $-e^{-i\phi_2}\sqrt{\gamma_{2R}\gamma_{3R}}+e^{i\phi_3}\sqrt{\gamma_{3R}\gamma_{4R}}$ $-e^{-i\phi_1}\sqrt{\gamma_{1L}\gamma_{2L}}-e^{-i(\phi_1+\phi_2+\phi_3)}\sqrt{\gamma_{1L}\gamma_{4L}}$ $+e^{i\phi_2}\sqrt{\gamma_{2L}\gamma_{3L}}-e^{-i\phi_3}\sqrt{\gamma_{3L}\gamma_{4L}}]/2i$

with

$$\Gamma_j = \Gamma_{jR} + \Gamma_{jL}, \qquad \text{for } j = A, B \tag{2.34}$$

$$\Gamma_{\rm coll} = \sqrt{\Gamma_{A,R}\Gamma^*_{B,R}} + \sqrt{\Gamma_{A,L}\Gamma^*_{B,L}}, \tag{2.35}$$

where * denotes complex conjugate.

The procedure used in these examples follows the SLH scheme depicted in Fig. 2.2(c), and it is the same used in Paper A, where we generalize it to a setup

of an arbitrary number of atoms with an arbitrary number of coupling points to the waveguide, and for any chirality of the coupling.

2.3 Chiral interfaces and applications

In general, we say that atoms couple *chirally* to a waveguide when their bare relaxation rate (the relaxation rate before any interference effects are taken into account) is generally different towards the right and left directions, i.e., $\gamma_R \neq \gamma_L$. Consequently, there are two limiting cases: the *bidirectional* or *nonchiral* case, where atoms couple symmetrically to the right and left ($\gamma_R = \gamma_L$), and the *unidirectional* or *cascaded* case, where atoms couple to modes propagating in only one direction (e.g., $\gamma_L = 0$).

Chirality emerges naturally in optical nanofibers when light is strongly transversely confined [51–53] and it is also achievable in atomic waveguides [54] and in microwave waveguides by using circulators [55–59], sawtooth lattices [60], or entangled states between quantum emitters [28]. Even beyond photonic reservoirs, other architectures with phononic [61–64] and magnonic waveguides [64–66] have been proposed to realize chiral coupling.

Chiral quantum networks have been increasingly attracting interest in recent years [67–76] since they have immediate applications in quantum information processing. With two-level emitters representing stationary qubits, and photons as 'flying qubits' for distributing quantum information in a quantum network, the chiral light-matter coupling enables photons to be routed in between the nodes. In particular, it has been shown how this coupling can be harnessed to transfer quantum states between qubits and to manipulate stabilizer codes for quantum error correction [27].

As a simple example, consider the setting in Fig. 2.2(a) with all $\gamma_L = 0$, and with the emitter on the left in an arbitrary superposition $c_g \left|g\right\rangle_A + c_e \left|e\right\rangle_A$ (defined by the complex coefficients c_g and c_e) and the emitter on the right in the ground state $\left|g\right\rangle_B$. Then the chiral setting could enable the quantum-state transfer $(c_g \left|g\right\rangle_A + c_e \left|e\right\rangle_A) \left|g\right\rangle_B \rightarrow \left|g\right\rangle_A (c_g \left|g\right\rangle_B + c_e \left|e\right\rangle_B)$, whereby an arbitrary superposition stored in emitter A is mapped to emitter B. Chiral coupling serves here to convert the first qubit to a rightward-propagating photonic qubit, and to increase the chance of reabsorption of this photon by the second qubit.

Let us take now the case of entanglement between emitters. On the one hand, even the slightest directionalities in the couplings have been shown to improve the maximum entanglement achievable as compared to nonchiral systems [68], while on the other hand, chirality can destroy collective emission effects. Consider the spontaneous emission of an ensemble of two-level emitters. Owing to the fact that all emitters are coupled to the same bath, the emission differs strongly from that of independent emitters—an effect referred to as sub- or super-radiance [77]. For instance, for bidirectional coupling, two small atoms can share a single excitation that is prevented from decaying by destructive interference between coupling points. This subradiant behavior, however, is not

possible if the atoms are coupled to a unidirectional waveguide, where the symmetry is broken and only one of the atoms "knows" about the presence of the other [71]. Interestingly, we found in Paper A that giant atoms in the nested configuration (i.e., where the coupling points of atom B are situated between the points of atom A—see Fig. 1.2(b)) preserve the symmetry and thus exhibit this subradiant behavior for any chirality of the coupling.

To get around the lack of subradiance for small atoms in chiral waveguides, it was shown in Ref. [69] that one can coherently drive the system. In such a case, the diatomic ensemble evolves to a dynamic equilibrium between drive and dissipation where the stream of photons scattered from the first atom interferes destructively with the photons scattered from the second [71]. In Paper A, we showed that such a regime is also accessible for giant atoms.

2.4 Protection from decoherence

2.4.1 Subradiance

Let us delve into the aforementioned phenomenon of *subradiance* [77–80], i.e., the suppression of spontaneous emission by collective interference. We typically label a many-atom state as subradiant whenever it decays slower than the relaxation of each individual atom. A perfectly subradiant state—that which does not decay—is known as a *dark* state. In an atomic network, dark states $|D\rangle$ are nonradiative pure states which are annihilated by all collapse operators and are eigenstates of the multiatom Hamiltonian [67, 69, 70, 79, 81], i.e., they satisfy

$$\begin{aligned} &\mathcal{L}_R\,|D\rangle = \mathcal{L}_L\,|D\rangle = 0 \\ &H\,|D\rangle = \mu\,|D\rangle\,,\ \ \mu \in \mathbb{R}. \end{aligned} \tag{2.36}$$

By applying these conditions to the examples in Sec. 2.2.3 we find that, under certain conditions for γ_k, ϕ_k and ω_j, the possible dark states are $|+\rangle$ and $|-\rangle$, which are maximally entangled states with one atom being excited and the other being in the ground state[2]:

$$|\pm\rangle = \frac{1}{\sqrt{2}}(|eg\rangle \pm |ge\rangle). \tag{2.37}$$

The conditions for the existence of dark states in small atoms are well known, and have been studied since the discovery of superradiance by Dicke in 1954. Conversely, these conditions had not been derived before for giant atoms, until we did in Paper A. In fact, it was by applying the conditions from Eq. (2.36) that we found that, while most diatomic configurations (including small atoms)

[2]There is no universal nomenclature for these states, but rather common naming practice differs between fields. The plus state $|+\rangle$ is also commonly referred to as the *triplet* $|T\rangle$ or the *symmetric* $|s\rangle$ state, whereas the minus state $|-\rangle$ is also known as the *singlet* $|S\rangle$ or the *antisymmetric* $|a\rangle$ state. We follow the notation $|S/T\rangle$ in Paper A and the notation $|\pm\rangle$ in Paper B.

require the coupling to be bidirectional for dark states to exist, i.e., $\gamma_R = \gamma_L$, the nested setting does not.

While collective emission phenomena have always been of interest to the quantum-optics community, subradiance is receiving a recently renewed interest in the context of quantum technologies: being able to access and harness dark states is a key ingredient in the development of quantum memories [82–84] and in the robust distribution of information in scalable quantum networks with quantum repeaters [85, 86].

2.4.2 Decoherence-free interaction

Subradiance offers a way of protecting atoms against decoherence only when the atoms are in the dark state. A much more robust way of protecting the atoms is achieved by braided GAs through the so-called *decoherence-free interaction* (DFI), which is independent of the states of the GAs, meaning that the entire Hilbert space of the atomic ensemble is protected from decoherence.

As mentioned in the Introduction, this is one of the most promising properties of GAs and a feature of great potential in quantum computing applications, a field which is currently largely limited by quantum decoherence and dissipation.

Waveguide-mediated DFI between two atoms A and B takes place when the interference from their coupling points suppresses both the individual and collective relaxation rates ($\Gamma_j, \Gamma_{\text{coll}} = 0 \ \forall j \in \{A, B\}$) while maintaining their exchange interaction ($g \neq 0$). Let us see when that happens.

By definition, an atomic ensemble does not decohere into the waveguide when the individual decay rate of each atom is zero, i.e., $\Gamma_j = 0 \ \forall j$. From the expressions in Table 2.1 for braided atoms, this implies that an excitation acquires a phase $\pi \pmod{2\pi}$ between the coupling points of atom j [see Fig. 2.3(a)], or equivalently, that the coupling points are separated by half the

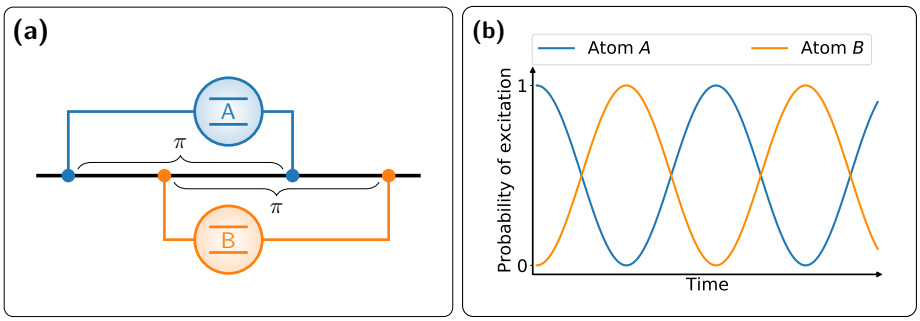

Figure 2.3: (a) Two braided giant atoms with the coupling points of each atom separated by a phase shift of $\pi \pmod{2\pi}$, which is the distance that allows them to interact without decohering. (b) Excitation exchange between two atoms arranged in the setup from (a), showing a decoherence-free interaction.

excitation's wavelength, $\lambda/2 \pmod{\lambda}$. For this particular distance, the emission from each atom's connection points interferes destructively, making the sum over all atoms zero and thus preventing collective decay ($\Gamma_{\text{coll}} = 0$). In separate and nested atoms, the connection points of atom B are consecutive, so the emission between them cancels the interaction ($g = 0$) when $\Gamma_B = 0$. Unlike these topologies, braided atoms have the particularity that no consecutive points belong to the same atom, allowing a non-zero exchange interaction [see Table 2.1]. As depicted in Fig. 2.3(b), this implies that an excitation can be released from atom A to be reabsorbed by atom B and vice versa, in a perpetual loop.

DFI was first described in Ref. [33] in 2018 and we showed that it holds for waveguides of any chirality in Paper A.

3 Structured waveguides

Structured waveguides are those which, contrary to continuous waveguides, have nontrivial dispersion relations, such as band edges and band gaps. A simple example is realized by a 1D array of coupled cavities, which creates a finite propagating band with a speed of light that is controlled by the tunnel coupling between neighboring cavities and thus can, in principle, be made arbitrarily small. This is why structured waveguides are also known as *slow-light waveguides* [87].

Many different platforms have been used to demonstrate phenomena arising from the interaction between an atom and a structured environment [88]. These include cold atoms coupled to either photonic crystal waveguides [89] or to an optical lattice [90, 91], as well as superconducting qubits coupled to either a microwave photonic crystal [92–94] or to a superconducting metamaterial [76, 95–98].

In general, a small atom coupled to a structured environment with its transition frequency tuned to the propagating band shows the typical exponential decay of spontaneous emission. Conversely, when the atom is detuned away from the band, i.e., when it is tuned to the band gap, it does not decay. This occurs because atom-photon bound states are formed in the band gaps, where photons become exponentially localized in the vicinity of the atoms, inhibiting their decay [87, 99–101]. Even at the band edge of the continuum of propagating modes, atoms show fractional decay due to the influence of bound states [102–104]. Furthermore, multiple atoms coupled to the same reservoir can interact through the overlap of their bound-state photonic wavefunctions [105–107]. These interactions can be tuned by modifying the frequencies of the atoms and their coupling strengths to the bath, which opens doors for applications in quantum computation and quantum simulation of many-body physics [108, 109].

Mathematically, a structured waveguide can be modeled with the same Hamiltonian as a continuous waveguide [Eq. (2.1)], but with a different dispersion relation. For example, in Paper B we use that the bath Hamiltonian rotating at the bath frequency can be expressed as $H_b = \sum_k \omega(k) a_k^\dagger a_k$, with

$$\omega(k) = -2J\cos(k), \tag{3.1}$$

where J is the hopping rate between coupled cavities. This describes a continuum of modes confined in an energy band $E \in [-2J, 2J]$, where the dispersion

is linear around the middle of the band [$\omega(\pm\pi/2+\varepsilon) = \pm 2J\sin(\varepsilon) \approx \pm 2J\varepsilon$] and parabolic close to the band edges [e.g., $\omega(\varepsilon) \approx -2J(1-\varepsilon^2/2)$]. In turn, this translates into a density of states

$$D(E) = \frac{1}{\pi\sqrt{4J^2 - E^2}}\Theta(2J - |E|), \tag{3.2}$$

that is nearly constant around the middle of the band (i.e., for energies $E \approx 0$) and diverges at the band edges ($|E/J| \approx 2$) [110]. This divergence leads to non-Markovian dynamics, such as the aforementioned appearance of atom-photon bound states and fractional decay at the band edges. This non-Markovianity prevents us from using the analytical tools described in Chapter 2, so in order to accurately describe the dynamics of the system, we instead resort to complex-analysis techniques based on Ref. [111].

3.1 Resolvent formalism

Let us consider a system with a total Hamiltonian $H = H_0 + H_{\text{int}}$, where H_0 is the "unperturbed" Hamiltonian for which the eigenstates and eigenenergies are known, and H_{int} represents the coupling between subspaces spanned by some of the unperturbed eigenstates. This could be the case of the Hamiltonian used in Chapter 2 [in Eq. (2.3)], where $H_0 = H_a + H_b$, i.e., the sum of the bare atom and bath Hamiltonians. There, we made many simplifications to be able to describe the atomic dynamics: we made the Born-Markov approximation, and we assumed a linear dispersionless bath with negligible travel time between components. With fewer simplifications, in many cases, we could take a perturbative approach to solve the dynamics. However, sometimes, a deeper understanding of certain physical phenomena requires going beyond perturbation theory and taking into account some effects of H_{int} to all orders.

For this type of problem, we resort to the so-called *resolvent formalism*, based on the definition of the *resolvent* $G(z) = 1/(z-H)$ of the Hamiltonian H, with $z \in \mathbb{C}$. The relation between the resolvent $G(z)$ and the unperturbed resolvent $G_0(z) = 1/(z-H_0)$ is an *algebraic* equation, much simpler to manipulate than the *integral* equation connecting the evolution operators $U(t) = \exp\{-iHt\}$ and $U_0(t) = \exp\{-iH_0t\}$. The matrix elements of $U(t)$ are then calculated from the matrix elements of $G(z)$ via a contour integral. Moreover, the analytical properties of $G(z)$ provide information about the different contributions to the dynamics.

3.1.1 From resolvent to evolution operator

The time-evolution operator $U(t,t')$ of the Hamiltonian $H = H_0 + H_{\text{int}}$ is the solution to the Schrödinger equation

$$i\frac{\mathrm{d}}{\mathrm{d}t}U(t,t') = (H_0 + H_{\text{int}})U(t,t'), \tag{3.3}$$

with the initial condition $U(t',t')=1$. In fact, the solution can be written as

$$U(t,t') = U_0(t,t') - i\int_{t'}^{t} d\tau U_0(t,\tau) H_{\rm int} U(\tau,t'), \tag{3.4}$$

where $U_0(t,t') = \exp\{-iH_0(t-t')\}$. Note that this expression is close to a convolution product, but not quite, since τ varies between t' and t. Fortunately, by introducing new operators, we can convert it to a true convolution product, which will transform into a simple product by Fourier transformation. We define

$$K_+(t,t') = U(t,t')\theta(t-t'); \qquad K_{0+}(t,t') = U_0(t,t')\theta(t-t'), \tag{3.5}$$

where $\theta(t-t')$ is the Heaviside function, equal to 1 for $t>t'$ and to 0 otherwise. With these operators, we can rewrite Eq. (3.4) as a true convolution:

$$K_+(t,t') = K_{0+}(t,t') - i\int_{-\infty}^{\infty} d\tau K_{0+}(t,\tau) H_{\rm int} K_+(\tau,t'). \tag{3.6}$$

We note that $K_+(t,t')$ satisfies the equation

$$\left(i\frac{\mathrm{d}}{\mathrm{d}t} - H\right) K_+(t,t') = \delta(t-t'), \tag{3.7}$$

which is why the operator $K_+(t,t')$ is sometimes called the *Green's function*. In fact, it is a *retarded* Green's function because it is non-zero only for $t>t'$. Conversely, we can define the *advanced* Green's function

$$K_-(t,t') = -U(t,t')\theta(t'-t), \tag{3.8}$$

which obeys the same evolution equation as K_+ but satisfies different boundary conditions.

We now introduce the Fourier transform of $K_+(t,t')$, which depends only on $t-t'$, so by redefining $t := t-t'$, we can write

$$K_+(t) = -\frac{1}{2\pi i}\int_{-\infty}^{\infty} dE\, e^{-iEt} G_+(E), \tag{3.9}$$

or, inversely,

$$\begin{aligned} G_+(E) &= -i\int_{-\infty}^{\infty} dt\, e^{iEt} \overbrace{K_+(t)}^{\exp\{-iHt\}\theta(t)} = -i\int_0^{\infty} dt\, e^{i(E-H)t} = \\ &= \lim_{\eta\to 0_+} -i\int_0^{\infty} dt\, e^{i(E-H+i\eta)t} = \lim_{\eta\to 0_+} \frac{1}{E-H+i\eta}, \end{aligned} \tag{3.10}$$

were η is a positive real number that tends to zero, and $G_+(E)$ is called *retarded*

propagator[1]. Similarly, the advanced Green's function and propagator satisfy

$$K_-(t) = -\frac{1}{2\pi i}\int_{-\infty}^{\infty} dE\, e^{-iEt} G_-(E), \tag{3.11}$$

$$G_-(E) = \lim_{\eta\to 0_+} \frac{1}{E - H - i\eta}. \tag{3.12}$$

Notice that, now, the integral from Eq. (3.6) becomes a simple product by Fourier transform, thus resulting in the algebraic equation

$$G_+(E) = G_{0+}(E) + G_{0+}(E) H_{\text{int}} G_+(E), \tag{3.13}$$

where G_{0+} is the retarded propagator associated with H_0.

The simple form of $G_\pm(E)$ suggests the introduction of the *resolvent* operator of the Hamiltonian H,

$$G(z) = \frac{1}{z - H}, \tag{3.14}$$

as a function of the complex variable z. Then, the retarded (advanced) propagator $G_+(E)$ $[G_-(E)]$ is simply the limit of $G(z)$ when z tends to the point E on the real axis, with a positive (negative) value of its imaginary part:

$$G_\pm(E) = \lim_{\eta\to 0_+} G(E \pm i\eta). \tag{3.15}$$

Finally, the time-evolution operator $U(t) = K_+(t) - K_-(t)$ is expressed by a contour integral of G(z):

$$\begin{aligned} U(t) =& \frac{1}{2\pi i}\int_{-\infty}^{\infty} dE\, e^{-iEt}[G_-(E) - G_+(E)] = \\ =& \frac{1}{2\pi i}\int_{C_+ + C_-} dz\, e^{-izt} G(z), \end{aligned} \tag{3.16}$$

where C_+ (C_-) is a line situated immediately above (below) the real axis and followed from right (left) to left (right). For $t > 0$ ($t < 0$), the contribution of C_- (C_+) is zero.

3.1.2 Singularities of the resolvent

It becomes patent from Eq. (3.16) that we can determine properties of $U(t)$ from the analytical properties of $G(z)$. In fact, the matrix elements of $G(z)$ are analytic functions of z in the whole complex plane except for the real axis, where they have two types of singularities:

- *Real poles*, located at the discrete eigenvalues of the Hamiltonian H, and

[1] Since K_+ and G_+ are interchangeable by Fourier transform, sometimes, it is K_+ which is referred to as the retarded propagator, and G_+ receives instead the name of retarded Green's function.

- *Branch cuts*, extending over the intervals corresponding to the continuous spectrum of H. A cut appears when the matrix elements of $G(z)$ do not tend to the same value when z tends from below or from above toward a point on the real axis, located on the cut.

Now, it is possible to analytically continue $G(z)$ from, e.g., the upper half-plane towards the lower half-plane, into the so-called *second Riemann sheet*. In this case, the continued function is not necessarily analytic outside the real axis and may have

- *Complex poles*, which describe *unstable* states of the system, i.e., states having a complex energy and characterized by exponential damping.

3.1.3 From level-shift operator to resolvent

The identity Eq. (3.13) can be applied to give the perturbative expansion of $G(z)$ in powers of V, and iterated to yield

$$\begin{aligned} G(z) &= G_0(z) + G_0(z)H_{\text{int}}G(z) = \\ &= G_0(z) + G_0(z)H_{\text{int}}G_0(z) + G_0(z)H_{\text{int}}G_0(z)H_{\text{int}}G_0(z) + \dots \end{aligned} \tag{3.17}$$

Then, the matrix elements of $G(z)$ between two eigenstates $\langle l|$ and $|m\rangle$ of H_0, with unperturbed energies E_l and E_m, read

$$\begin{aligned} G_{lm}(z) = &\frac{1}{z-E_l}\delta_{lm} + \frac{1}{z-E_l}H^{\text{int}}_{lm}\frac{1}{z-E_m} \\ &+ \sum_i \frac{1}{z-E_l}H^{\text{int}}_{li}\frac{1}{z-E_i}H^{\text{int}}_{im}\frac{1}{z-E_m} + \dots, \end{aligned} \tag{3.18}$$

where $|i\rangle$ are eigenstates of H_0, $G_{lm}(z) = \langle l|G(z)|m\rangle$, and $H^{\text{int}}_{im} = \langle i|H_{\text{int}}|m\rangle$. Note that this expression is quite simple, consisting only of products of matrix elements of H_{int} and of unperturbed energy denominators. In this way, we can regroup the terms where a denominator $1/(z-E_e)$ involving a particular unperturbed state $|e\rangle$ appears x times, and then formally sum the perturbation series. Let us take $l = m = e$. Then, the zero-order term in H_{int} of Eq. (3.18) is just $1/(z-E_e)$ and thus contains this denominator once. Meanwhile, the next terms in the expansion contain the denominator at least twice. If we require them to contain the denominator *only* twice, then we can express the sum as

$$\Sigma_e(z) = H^{\text{int}}_e + \sum_{i\neq e}\frac{1}{z-E_i}H^{\text{int}}_{ie} + \sum_{i\neq e}\sum_{j\neq e}H^{\text{int}}_{ei}\frac{1}{z-E_i}H^{\text{int}}_{ij}\frac{1}{z-E_j}H^{\text{int}}_{je} + \dots, \tag{3.19}$$

but we can generalize it to contain the denominator x times. In fact, it is sufficient to sum the contributions corresponding to different values of x to obtain

$$G_e(z) = \sum_{x=1}^{\infty}\frac{[\Sigma_e(z)]^{x-1}}{(z-E_e)^x} = \frac{1}{z-E_e}\sum_{x=0}^{\infty}\left[\frac{\Sigma_e(z)}{z-E_e}\right]^x = \frac{1}{z-E_e-\Sigma_e(z)}, \tag{3.20}$$

which is an exact expression for $G_e(z) = \langle e|G(z)|e\rangle$.

Projection of the resolvent

Equation (3.20) can also be derived using projection operators. Consider the subspace spanned by some eigenvectors $\{|a\rangle, |b\rangle, \ldots, |l\rangle\}$ of the unperturbed Hamiltonian H_0. If they are orthonormal, the projector onto the subspace is

$$P = |a\rangle\langle a| + |b\rangle\langle b| + \cdots + |l\rangle\langle l|. \tag{3.21}$$

The projector onto the complementary subspace is then $Q = 1 - P$. Since the subspaces are orthogonal, then $PQ = QP = 0$, and since the states $|a\rangle, |b\rangle, \ldots, |l\rangle$ are eigenstates of H_0, then $[P, H_0] = [Q, H_0] = 0$. From these two relations, we derive that

$$PH_0Q = QH_0P = 0. \tag{3.22}$$

Let us now take the definition of resolvent and manipulate it by multiplying on the right by P and on the left by P or Q:

$$\begin{aligned}
&G(z) = \frac{1}{z - H} \implies (z - H)G(z) = 1 \\
&\implies \begin{cases} P(z-H)\underbrace{(P+Q)}_{1}G(z)P = \underbrace{P^2}_{P} \\ Q(z-H)\overbrace{(P+Q)}^{1}G(z)P = \underbrace{QP}_{0} \end{cases} \\
&\implies \begin{cases} P(z-H)[PG(z)P + QG(z)P] = P \\ Q(z-H)[PG(z)P + QG(z)P] = 0 \end{cases} \\
&\implies \begin{cases} P(z-H)\underbrace{PP}_{P}G(z)P + P(z\underbrace{-H_0 - H_{\mathrm{int}}}_{-H})\underbrace{QQ}_{Q}G(z)P = P \\ Q(z\underbrace{-H_0 - H_{\mathrm{int}}}_{-H})\underbrace{PP}_{P}G(z)P + Q(z-H)\underbrace{QQ}_{Q}G(z)P = 0 \end{cases} \\
&\implies \begin{cases} P(z-H)P[PG(z)P] + \cancelto{0}{PQz} - \cancelto{0}{PH_0Q} - PH_{\mathrm{int}}Q[QG(z)P] = P \\ \cancelto{0}{QPz} - \cancelto{0}{QH_0P} - QH_{\mathrm{int}}P[PG(z)P] + Q(z-H)Q[QG(z)P] = 0 \end{cases}
\end{aligned} \tag{3.23}$$

We can solve the system of equations above for $PG(z)P$ by substitution of $QG(z)P$ to obtain

$$P\left[z - H_0 - H_{\mathrm{int}} - H_{\mathrm{int}}\frac{Q}{z - QH_0Q - QH_{\mathrm{int}}Q}H_{\mathrm{int}}\right]PG(z)P = P. \tag{3.24}$$

For this expression, we define the *level-shift operator* $\Sigma(z)$ as follows:

$$\Sigma(z) = H_{\mathrm{int}} + H_{\mathrm{int}}\frac{Q}{z - QH_0Q - QH_{\mathrm{int}}Q}H_{\mathrm{int}}, \tag{3.25}$$

whose perturbative expansion in powers of H_{int} reads

$$\Sigma(z) = H_{\text{int}} + H_{\text{int}}\frac{Q}{z-H_0}H_{\text{int}} + H_{\text{int}}\frac{Q}{z-H_0}H_{\text{int}}\frac{Q}{z-H_0}H_{\text{int}} + \dots. \tag{3.26}$$

Rewriting Eq. (3.24) in terms of the level shift operator [Eq. (3.25)] yields

$$PG(z)P = \frac{P}{z - PH_0P - P\Sigma(z)P}, \tag{3.27}$$

which generalizes equation Eq. (3.20). The form of Eq. (3.27) suggests that $P\Sigma P$ can be considered as a "Hamiltonian" (ignoring the dependence on z) in the subspace spanned by $\{|a\rangle, |b\rangle, \dots, |l\rangle\}$ being added to PH_0P and allowing us to determine the shifts of the perturbed levels relative to unperturbed levels. This is why $\Sigma(z)$ is called the *level-shift operator*.

3.2 Residue theorem

Before we move on to applying the resolvent formalism to a physical scenario, let us review one last concept from complex analysis: the residue theorem.

Consider a function $f(z)$ that has a pole of order m at $z = a$. Then by definition of a pole,

$$f(z) = \frac{A_{-m}}{(z-a)^m} + \frac{A_{-m+1}}{(z-a)^{m-1}} + \dots + \frac{A_{-1}}{(z-a)} + g(z), \tag{3.28}$$

where $g(z)$ is analytic near and at a, and the coefficient A_{-1} is called the *residue* $\text{Res}(f, a)$ of the function $f(z)$ relative to the pole a [112]. Formally,

$$\text{Res}(f, a) = A_{-1} = \lim_{z\to a}\left(\frac{1}{(m-1)!}\left(\frac{\mathrm{d}}{\mathrm{d}z}\right)^{m-1}[(z-a)^m f(z)]\right). \tag{3.29}$$

It follows from the above definition that, if a is a *simple* pole of $f(z)$, the residue of $f(z)$ at that pole is $\lim_{z\to a}[(z-a)f(z)]$.

The *residue theorem* states that if $f(z)$ is analytic throughout a contour C and its interior except at a number of poles $a_1, \dots, a_n$ inside the contour, then

$$\frac{1}{2\pi i}\int_C f(z)dz = \sum_{j=1}^{n}\text{Res}(f, a_j)\,\text{wind}(C, a_j), \tag{3.30}$$

where $\text{wind}(C, a_j)$ is the winding number of C around a_j [112]. Note that $\text{wind}(C, a_j) = 0$ if a_j falls outside the contour.

3.3 Example: a giant atom in a structured waveguide

Consider the simplest setup from Paper B: a single giant atom with two connection points coupled to a structured waveguide, and suppose we want to find

the time evolution of the atomic population. We can start by writing the total Hamiltonian as the sum $H = H_0 + H_{\text{int}}$, with

$$H_0 = \Delta\sigma^+\sigma^- + \sum_k \omega(k) a_k^\dagger a_k \tag{3.31}$$

$$H_{\text{int}} = \frac{g}{\sqrt{N}} \sum_k \left[\left(e^{ikn_1} + e^{ikn_2} \right) a_k \sigma^+ + \text{H.c.} \right], \tag{3.32}$$

where Δ is the detuning of the atom with respect to the bath frequency, $\sigma^\pm$ denote the atomic ladder operators, $a_k^\dagger, a_k$ are the creation and annihilation operators of the cavity modes, $\omega(k)$ is given by the dispersion relation from Eq. (3.1), N is the number of coupled cavities conforming the bath, and n_p denotes the position of the p-th coupling point. Note that we have applied the RWA directly on the Hamiltonian, which requires that the atomic and bath resonant frequencies are much larger than the coupling strength g, and, as explained in Sec. 2.1.1, will not yield an accurate value of the Lamb shifts.

In the single-excitation subspace, the eigenstates of the unperturbed Hamiltonian H_0 consist of an atomic excitation $|e\rangle := |e, 0\rangle$, and a photonic excitation in mode $k \in [-\pi, \ldots, \pi - \frac{2\pi}{N}]$, $|k\rangle := |g, k\rangle$. It is the interaction term H_{int} that couples the subspace $\{|e\rangle\}$ with $\{|k\rangle\}$. We can then define the projector $P = |e\rangle\langle e|$ and its complementary $Q = \sum_k |k\rangle\langle k|$, and use the techniques described in the previous section, but in inverse order: we will first derive the matrix elements of the level-shift operator and, from there, we will deduce the resolvent and the time-evolution operator.

Let us start with the perturbative expansion of the level-shift operator in powers of H_{int} shown in Eq. (3.26), truncated to second order:

$$\Sigma(z) = H_{\text{int}} + H_{\text{int}} \frac{Q}{z - QH_0Q - QH_{\text{int}}Q} H_{\text{int}} \approx H_{\text{int}} + H_{\text{int}} \frac{Q}{z - H_0} H_{\text{int}}. \tag{3.33}$$

It is nontrivial to see why this truncation is justified, so let us elucidate. Assume the eigenstate $|e\rangle$ of H_0 is well isolated from all the other discrete eigenstates of H_0. Let us examine Eq. (3.19) near $z = E_e$, which is where $G_e(z)$ [see Eq. (3.20)] takes on the most important values. All the energy denominators involved in the expansion of $\Sigma_e(z)$ are large because the other discrete energies of H_0 are assumed to be far from E_e. Nevertheless, even if E_e falls within the continuous spectrum of H_0, the sums over the intermediate states associated with this continuous spectrum involve delta functions and principal parts which do not lead to any divergnce. Thus, if H_{int} is small compared to H_0, the perturbative series Eq. (3.19) is rapidly convergent and it is completely valid to approximate $\Sigma_e(z)$ by retaining only a finite number of terms.

It is important to remark that a perturbative approximation for $\Sigma_e(z)$ does *not* correspond to a perturbative approximation for $G_e(z)$, since $G_e(z)$ obtained by truncation of $\Sigma_e(z)$ still contains arbitrarily high powers of H_{int}. In other words, the truncation in Eq. (3.33) is equivalent to making a partial resummation of the perturbation theory.

Now, we can go back to the level-shift operator in Eq. (3.33) and calculate the matrix element $\Sigma_e(z) = \langle e|\Sigma(z)|e\rangle$, known as the *self-energy* of the atom:

$$\begin{aligned}\Sigma_e(z) &= \cancelto{0}{\langle e|H_{\text{int}}|e\rangle} + \sum_k \langle e|\, H_{\text{int}} \frac{|k\rangle\langle k|}{z - H_0} H_{\text{int}}\, |e\rangle = \\ &= \frac{g^2}{N} \sum_k \frac{(e^{ikn_1} + e^{ikn_2})(e^{-ikn_1} + e^{-ikn_2})}{z - \omega(k)} = \\ &= \frac{2g^2}{N} \sum_k \frac{1 + \cos(k(n_2 - n_1))}{z - \omega(k)}. \end{aligned} \tag{3.34}$$

Henceforth, we use the dispersion relation $\omega(k) = -2J\cos(k)$ and that the distance between coupling points is $d = n_2 - n_1$. In the continuum limit, i.e., when $N \to \infty$, the sum over k becomes an integral: $\sum_k \frac{2\pi}{N} \to \int_k dk$. Therefore, we can write the self-energy like

$$\begin{aligned}\Sigma_e(z) &= \frac{g^2}{\pi} \int_{-\pi}^{\pi} \frac{1 + \cos(kd)}{z + 2J\cos(k)} dk = \\ &= \frac{g^2}{\pi} \int_{-\pi}^{\pi} \frac{dk}{z + 2J\cos(k)} + \frac{g^2}{\pi} \int_{-\pi}^{\pi} \frac{e^{ikd}}{z + 2J\cos(k)} dk, \end{aligned} \tag{3.35}$$

where, in the second integral, we have substituted the cosine for an exponential because odd functions do not contribute to the integral. Now, we can introduce the change of variable $\tilde{z} = e^{ik}$ such that $2\cos(k) = \tilde{z} + \tilde{z}^{-1}$ and $dk = -i\tilde{z}^{-1}d\tilde{z}$, and integrate over the unit circle:

$$\begin{aligned}\Sigma_e(z) &= -\frac{ig^2}{\pi} \oint \frac{d\tilde{z}}{z\tilde{z} + J\tilde{z}^2 + 1} - \frac{ig^2}{\pi} \oint \frac{\tilde{z}^d d\tilde{z}}{z\tilde{z} + J\tilde{z}^2 + 1} = \\ &= -\frac{ig^2}{\pi J} \oint \frac{(1 + \tilde{z}^d)d\tilde{z}}{(\tilde{z} - f_+)(\tilde{z} - f_-)}, \end{aligned} \tag{3.36}$$

where the function $(1+\tilde{z}^d)$ is an entire function, i.e., it does not have singularities in the complex plane, and the poles of the denominator are

$$f_\pm(z) = \frac{-z \pm \sqrt{z^2 - 4J^2}}{2J}. \tag{3.37}$$

Applying the residue theorem [Eq. (3.30)], we obtain that

$$\oint \underbrace{\frac{(1 + \tilde{z}^d)}{(\tilde{z} - f_+)(\tilde{z} - f_-)}}_{F(\tilde{z})} d\tilde{z} = 2\pi i \sum_\pm \text{Res}(F, f_\pm)\, \text{wind}(S^1, f_\pm) \tag{3.38}$$

where the residues are

$$\begin{aligned}\text{Res}(F, f_\pm) &= \lim_{\tilde{z} \to f_\pm} (\tilde{z} - f_\pm) F(\tilde{z}) = \frac{1 + f_\pm^d}{f_\pm - f_\mp} = \\ &= \frac{\pm J}{\sqrt{z^2 - 4J^2}} \left[1 + \left(\frac{-z \pm \sqrt{z^2 - 4J^2}}{2J}\right)^d\right], \end{aligned} \tag{3.39}$$

and the winding number is zero for the poles that fall outside of the unit circle S^1, i.e.,

$$\mathrm{wind}(S^1, f_+) = \begin{cases} 1 & \mathrm{Re}\{z\} > 0 \\ 0 & \mathrm{Re}\{z\} < 0 \end{cases}, \qquad \mathrm{wind}(S^1, f_-) = \begin{cases} 0 & \mathrm{Re}\{z\} > 0 \\ 1 & \mathrm{Re}\{z\} < 0. \end{cases} \tag{3.40}$$

Therefore, we can insert the results of the residue theorem into Eq. (3.36) to obtain the final expression of the self-energy:

$$\Sigma_e(z) = \mathrm{sgn}(\mathrm{Re}\{z\}) \frac{2g^2}{\sqrt{z^2 - 4J^2}} \left[1 + \left(\frac{-z + \mathrm{sgn}(\mathrm{Re}\{z\})\sqrt{z^2 - 4J^2}}{2J} \right)^d \right]. \tag{3.41}$$

According to Eq. (3.20), the resolvent matrix element corresponding to the excited state of the atom is then

$$G_e(z) = \frac{1}{z - \Delta - \Sigma_e(z)}, \tag{3.42}$$

with Δ being the atom-cavity detuning. Lastly, we can express the probability amplitude of an initially excited GA, for $t > 0$, as follows from Eq. (3.16):

$$C_e(t) = -\frac{1}{2\pi i} \int_C G_e(E + i0^+) e^{-iEt}\, dE, \tag{3.43}$$

where the contour C is shown in Fig. 3.1.

The derivation presented here is used in Paper B for a single giant atom. For two atoms, the procedure is similar, but a bit trickier, since the $G(z)$ is not diagonal in the basis $\{|eg\rangle, |ge\rangle\}$ (where one atom is excited and the other one is in the ground state), thus making it harder to calculate the matrix elements. An outline of the procedure to follow in such a case is presented in the Appendix of Paper B.

3.3.1 Contributions to the probability amplitude

In Fig. 3.1, we illustrate the different singularities of the resolvent that we introduced in Sec. 3.1.2 applied to the example of a giant atom coupled to a structured waveguide:

- **Branch cuts.** They are introduced by the dispersion relation into the self-energy [Eq. (3.41)] through the presence of the square root. It implies we cannot close directly the integral with a semicircle in the lower half-plane. By defining the branch cuts at the band edges, we can continuously close the contour by taking a detour around them.

- **Real poles.** They are isolated poles of the resolvent [Eq. (3.42)] that fall outside the continuum, i.e., they satisfy $z - \Delta - \Sigma_e(z) = 0$ and $|z| > 2J$. They correspond to the atom-photon bound states.

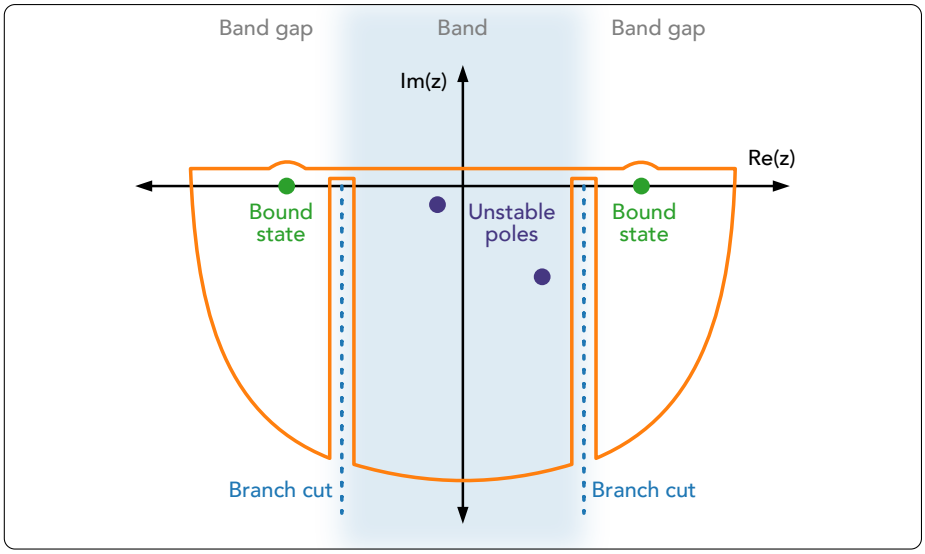

Figure 3.1: Contour of the integral in Eq. (3.43), with contributions from the poles of the resolvent [Eq. (3.42)] and the branch cuts at the band edges ($|\mathrm{Re}(z)/J| = 2$). Figure extracted from Paper B and inspired by Ref. [110].

- **Complex or unstable poles.** They arise from the analytical continuation of $G(z)$ into the second Riemann sheet, i.e., the surface contained between the branch cuts, which can be done by replacing $\sqrt{\dots}$ with $-\sqrt{\dots}$ in $\Sigma_e(z)$ [Eq. (3.41)]. They satisfy $|\mathrm{Re}\{z\}| < 2J$ and are responsible for the spontaneous emission of the atom into the bath when $\Delta \in [-2J, 2J]$.

Then, the probability amplitude $C_e(t)$ can be calculated as a sum of the different contributions [110]:

$$C_e(t) = \sum_{\alpha \in \substack{\text{branch} \\ \text{cuts}}} C_\alpha(t) + \sum_{\beta \in \text{poles}} R_\beta e^{-iz_\beta t}, \tag{3.44}$$

where C_α has the form of Eq. (3.43) and R_β is the residue of the real and unstable poles that we obtain through the residue theorem and that gives the overlap of the initial wave function with the poles, i.e.,

$$R_\beta = \left. \frac{1}{1 - \partial_z \Sigma_e(z)} \right|_{z=z_\beta}. \tag{3.45}$$

In particular, the contribution of the detour around the branch cuts to

Eq. (3.44) can be written as

$$\begin{aligned} C_e(t)\Big|_{\mathrm{UBC}} &= -\frac{1}{2\pi i}\int_{-\infty}^{0} G_e(2J+iy)e^{-i(2J+iy)t}\,dy \\ &\quad -\frac{1}{2\pi i}\int_{0}^{-\infty} G_e^{\mathrm{2RS}}(2J+iy)e^{-i(2J+iy)t}\,dy, \\ C_e(t)\Big|_{\mathrm{LBC}} &= -\frac{1}{2\pi i}\int_{-\infty}^{0} G_e^{\mathrm{2RS}}(-2J+iy)e^{-i(-2J+iy)t}\,dy \\ &\quad -\frac{1}{2\pi i}\int_{0}^{-\infty} G_e(-2J+iy)e^{-i(-2J+iy)t}\,dy, \end{aligned} \tag{3.46}$$

where UBC and LBC denote upper and lower branch cut, respectively, and the superscript 2RS stands for second Riemann sheet.

Finally, we note that the poles and the branch-cut integrals can be solved numerically, thus allowing us to simulate the exact dynamics of the atom through Eq. (3.44).

3.4 Non-Markovian effects

Unlike in Chapter 2 for continuous waveguides, here we have not made the Markovian approximation at any point in our derivation, thus allowing us to discern non-Markovian behaviors when computing the time evolution of the atoms.

3.4.1 Unstable poles and branch cuts

In the previous section, we mentioned that the unstable poles of the resolvent are responsible for the spontaneous emission of the atoms into the bath when the atoms are tuned to the band.

Within the Markovian approximation, we assume that the coupling g is sufficiently weak such that $\Sigma_e(E+i0^+) \approx \Sigma_e(\Delta)$ [110]. Then, $C_e(t)$ can be easily solved applying the residue theorem around the pole $z = \Delta + \Sigma_e(\Delta)$ to yield $C_e(t) \approx \exp\{-i[\Delta + \Sigma_e(\Delta)]t\}$. It then follows that we can split $\Sigma_e(\Delta)$ into its real and imaginary parts, and identify the frequency-dependent Lamb shift $\delta_e(\Delta) = \mathrm{Re}\{\Sigma(\Delta)\}$ and the decay rate $\Gamma_e(\Delta) = -2\,\mathrm{Im}\{\Sigma(\Delta)\}$ as follows [111]:

$$\Sigma_e(\Delta) = \delta_e(\Delta) - i\frac{\Gamma_e(\Delta)}{2}. \tag{3.47}$$

Moreover, using the same approximation for $C_k(t)$ shows that the modes dominating the emission will be those satisfying $\omega(k) \approx \Delta$ [110].

Now, solving the exact pole equation of the resolvent as we outlined in Sec. 3.3 allows us to go beyond the Markov approximation and obtain a more accurate profile of the decay rate $\Gamma_e(\Delta)$. In fact, we can depict such a profile

by plotting both $\Gamma_e(\Delta) = -2\,\mathrm{Im}\{\Sigma(\Delta)\}$ (Markov) and $\Gamma_e(\Delta) = -2\,\mathrm{Im}\{z\}$ with z being the poles (beyond Markov), and clearly illustrate where the Markovian approximation breaks down. This is what we did in Paper B, and we showed that, as expected, the middle of the band falls in the Markovian regime, whereas the approximation breaks down close to the band edges.

Around the band edges, the branch-cut contributions to the probability amplitude are also more prominent than at the band center [110, 113]. However, they never take prevalence over the contributions from the poles, and they are only relevant at the initial time of decay (small t), quickly decaying due to the exponential in Eq. (3.46). Therefore, although we include these contributions in both analytical and numerical results of Paper B, the branch cuts are not responsible for any of the main phenomena studied in that manuscript.

3.4.2 Time delay

Another consequence of solving the atomic dynamics exactly is that we observe time-delay effects, which arise from the time it takes an excitation to travel between two points through the bath. These become relevant in processes governed by interference effects, such as subradiance and DFI.

In Paper B, we talk about subradiance not as the collective interference effect between two atoms, but as the destructive interference between two coupling points of the *same* atom. While that may very well be abuse of language, we believe it is justified since, in the single-excitation regime, the subradiance that takes place between two small atoms is identical to that of a giant atom with two coupling points. In any case, the perfect subradiance is deteriorated by losses to the bath during the time it takes for the interference to build up, i.e., the time it takes for the excitation to travel between coupling points. The deterioration of the atomic population is exponentially worse with increasing distance between coupling points.

Similarly, DFI between two braided giant atoms is also worsened by the delay of the interference, in addition to an exponential deterioration over time caused by the imaginary part of the unstable poles that sustain the interaction.

3.4.3 Fractional and other anomalous decay

As mentioned at the beginning of Chapter 3, atom-photon bound states (real poles of the resolvent) cause fractional decay at the band edges [102–104]. This occurs because the spontaneous emission of the atom is counteracted by the hybridization with the bound state, prompting an initial exponential decay with a few beatings that stabilizes to a nonzero value of the population ($|C_e(t \to \infty)|^2 \neq 0$).

Similarly, other anomalous decay takes place due to the existence of other poles. As we described in Sec. 3.4.1, in the Markovian regime, the atomic population of each atom is dominated by a single pole. However, with increasing distance between coupling points and increasing detuning from the middle of

the band ($|\Delta| < 2J$), more poles appear and, as their contributions become relevant, the population exhibits beatings and other anomalous behavior. This can be understood through Eq. (3.44), where the atomic probability amplitudes become a sum of exponential functions with different frequencies and weights. In fact, this is the very reason why DFI is destroyed close to the band edges, as we showed in Paper B.

4 Paper overview

In this chapter, we give an overview of the two appended papers upon which this thesis is based. Both papers are theoretical studies about the coupling of GAs to a certain environment and how that bath mediates the dynamical interaction between several GAs.

4.1 Paper A – Chiral quantum optics with giant atoms

In Paper A, we studied the interaction between atoms chirally coupled to a continuous open waveguide. We began by considering simple setups: two small atoms and two giant atoms with two coupling points each, in all the possible configurations of coupling points (separate, nested, and braided). For simplicity, we first assumed all points had the same coupling strength γ, but that it was different in each propagation direction, i.e., $\gamma_R \neq \gamma_L$.

By using SLH formalism, we derived a master equation to model their dynamics in the same way we did in Sec. 2.2.3.

We showed that braided giant atoms can interact without decohering regardless of the chirality of their coupling to the waveguide, and we derived the phase-shift conditions for that to occur, as explained in Sec. 2.4.2. With this, we demonstrated that the most robust way we know of protecting against decoherence was also robust against variations in directionality.

In the spirit of searching for ways to protect the atoms against decoherence, we also investigated dark states. We derived conditions for the existence of such states in undriven atomic ensembles, as outlined in Sec. 2.4.1. We showed that, unlike small atoms, nested giant atoms allow for perfect subradiance regardless of the chirality of their coupling.

We also went further and looked at the effects of coherently driving the system, since it is known [69] that this is a way to get around the absence of dark states for small atoms in chiral settings. We showed that, when a drive is considered, two giant atoms evolve to a dynamic equilibrium between drive and dissipation, where the scattered photons from the first atom interfere destructively from those of the second atom. This is the same behavior as

for two small atoms, except that we showed giant atoms can populate these driven-dissipative dark states faster.

Finally, we generalized all results to an arbitrary number of atoms with an arbitrary number of coupling points, and presented interesting configurations that could be used to harness DFI and dark states.

4.2 Paper B – Interaction between giant atoms in a one-dimensional structured environment

In Paper B, we studied giant atoms coupled to a structured waveguide, modeled as an array of evenly spaced coupled cavities with nearest-neighbor interaction, and with the dispersion relation introduced at the beginning of Chapter 3.

First, we considered a single giant atom, and from the system-bath Hamiltonian, we characterized the energy spectrum of the total system and the wave function of the bound states. Then, we looked into the dynamics of the atom, both through numerical simulations and through complex-analysis techniques, as detailed in Sec. 3.3. In particular, we showed how the interference between coupling points of the atom affects its relaxation, and how the poles of the resolvent provide a much more accurate description of the decay rate than the Markovian prediction does close to the band edges. We related those results to the time evolution of the atomic population, when the atom is tuned to different regions of the band structure.

With a single atom fully characterized, we modeled the interaction between two giant atoms and analyzed the differences between tuning the atoms to the continuum and to the band gap. Within the band, we showed that DFI is best in the continuous-waveguide case, i.e., in the middle of the band, but also possible for other detunings. We also demonstrated, through different metrics, how DFI deteriorates exponentially with increasing distance between the coupling points. By mapping the DFI mechanism to the singularities of the resolvent introduced in Sec. 3.1.2, we dissected the dynamics into different contributions and showed the significance of time delay and other non-Markovian effects. Lastly, we identified DFI as the multiple-giant-atom analogue of subradiance.

In the band gap, we showed that GAs can interact through the overlap of bound states in the same way small atoms do. That raised the question: what kind of interaction is best—giant atoms inside the band (DFI), giant atoms outside the band (bound-state overlap), or small atoms outside the band (bound-state overlap)? We concluded that the answer depends on three parameters: the coupling strength, the distance between coupling points, and the detuning of the atoms from the cavities. In particular, giant atoms can provide an advantage over small atoms in some regions of the parameter space, for instance, when restricting the maximum coupling strength achievable per coupling point. We also found that there is a trade-off between good population exchanges and high

interaction rates. All in all, while for some parameters giant atoms can interact more strongly and over longer distances than small atoms, the preference of a giant-atom design over a small-atom design should depend on the experimental constraints and the intended application.

5 Outlook

The appended papers upon which this thesis is built consider setups that are simplifications of real-life systems and thus carry limitations in how well they actually represent them. In this final chapter, we discuss those limitations and how to overcome them in the future.

In both articles and throughout this thesis, we considered giant atoms as two-level systems. While this is sometimes a good approximation, it is not always the case, for instance, for superconducting qubits with small anharmonicity [9, 114]. It would therefore be interesting to study the atoms as three-level Ξ, Λ, V, or Δ systems, since this is a regime that has barely been explored in giant atoms [24, 26, 115], in particular with regards to adiabatic-passage techniques [116–118].

Another limitation that both appended papers share is the assumption of the single-excitation regime, i.e., that there is at most one photon in the system. In fact, in Paper A we do consider the possibility of both atoms being excited simultaneously, but we never actually populate that state. Going beyond the single-excitation subspace would allow us to study collective emission effects, such as superradiant bursts [119, 120] and multi-excitation subradiant states [121], as well as multiphoton bound states in structured environments [87, 98].

In the same way as we could extend the dimensionality of the excitation space, we could also extend the dimensionality of the reservoir. In fact, we are currently investigating two-dimensional structured baths, which have been shown to foster unconventional quantum optical behavior [25, 110, 122].

For structured waveguides, it would also be interesting to look at more elaborate band structures [88, 123], which can be engineered by tuning the hopping rate J between neighboring cavities. For instance, alternating a low hopping rate J_1 with a higher one $J_2 > J_1$, which is achieved by spacing the cavities further apart (J_1) or closer together (J_2), represents the Su-Schrieffer-Heeger (SSH) model of a photonic topological insulator [76, 124]. These kind of interfaces that support richer band structures have been shown to lead to nontrivial topological properties [76, 113, 125–128]. Moreover, when trying to match the theoretical predictions to experimental data, it could be a good idea to extend the current model of the bath to include next-to-nearest-neighbor interaction, since it it has been proven to be necessary in some architectures [98].

One more assumption we made in both appended papers is that we neglected external sources of decoherence, such as coupling to other baths, in order to

single out the reservoir we were interested in studying. However, in experiments, these other sources might become unavoidable and/or non-negligible in some instances, e.g., when the rate of interaction between atoms is low, or when the atoms are very long-lived. Thus, a more realistic approach would be needed when investigating applications that rely on the atoms not decaying too fast, such as the implementation of quantum gates.

Finally, from a more applied standpoint, it would be exciting to conceive more concrete proposals and turn more giant-atom theory into experiment. For instance, let us take the model presented in Paper A, which is ready to be implemented using superconducting qubits coupled to a transmission line with circulators inserted to provide the chirality [56]. Problems arise in the implementation due to the limitations of currently available circulators: they either are lossy and off-chip, and therefore they require additional space in the experimental setup, or they are on-chip and require active control by dynamic modulation [58, 129]. In recent years, a few proposals for passive on-chip superconducting circulators have emerged [59], interestingly two of them involving giant atoms [130] and giant molecules [29]. However, since each come with their own set of limitations, it remains to be seen whether giant atoms will be the solution to nonreciprocal chiral routing.

In the context of continuous waveguides, many other giant-atom features can be exploited. As shown in Ref. [12], the decoherence-free interaction enables the creation of any quantum many-body state among the atoms, since the interaction can be used to form a universal set of quantum gates. The interaction of this many-body system with the environment represented by the waveguide can then be turned on and off for quantum simulations by controlling the phase shifts ϕ_j in the setup, e.g., by tuning the atomic frequencies. Similarly, the universal gate set can be used to create entangled states that then are released into the waveguide for quantum communication or measurement-based quantum computing.

On the other hand, with the technology available today, the setup from Paper B is readily implementable with superconducting qubits coupled to either a microwave photonic crystal [92–94] or to a superconducting metamaterial [76, 95–98]. This platform has great potential for quantum gate implementation [98] and quantum simulation [32], as it has been recently demonstrated by an experiment simulating the Bose-Hubbard model [108], as well as by a proposal for the implementation of variational quantum algorithms [109].

Bibliography

[1] J. P. Dowling and G. J. Milburn, "Quantum technology: The second quantum revolution", Philosophical Transactions of the Royal Society A: Mathematical, Physical and Engineering Sciences **361**, 1655–1674 (2003).

[2] I. Georgescu and F. Nori, "Quantum technologies: an old new story", Physics World **25**, 16–17 (2012).

[3] M. A. Nielsen and I. L. Chuang, *Quantum Computation and Quantum Information* (Cambridge University Press, 2010).

[4] I. M. Georgescu, S. Ashhab, and F. Nori, "Quantum simulation", Reviews of Modern Physics **86**, 153 (2014).

[5] N. Gisin and R. Thew, "Quantum Communication", Nature Photonics **1**, 165–171 (2007).

[6] C. Degen, F. Reinhard, and P. Cappellaro, "Quantum sensing", Reviews of Modern Physics **89**, 035002 (2017).

[7] A. S. Sheremet, M. I. Petrov, I. V. Iorsh, A. V. Poshakinskiy, and A. N. Poddubny, "Waveguide quantum electrodynamics: collective radiance and photon-photon correlations", arXiv:2103.06824 [quant-ph] (2021).

[8] M. V. Gustafsson, T. Aref, A. F. Kockum, M. K. Ekström, G. Johansson, and P. Delsing, "Propagating phonons coupled to an artificial atom", Science **346**, 207–211 (2014).

[9] J. Koch, T. M. Yu, J. Gambetta, A. A. Houck, D. I. Schuster, J. Majer, A. Blais, M. H. Devoret, S. M. Girvin, and R. J. Schoelkopf, "Charge-insensitive qubit design derived from the Cooper pair box", Physical Review A **76**, 042319 (2007).

[10] S. Datta, *Surface Acoustic Wave Devices* (Prentice-Hall, 1986).

[11] A. Frisk Kockum, P. Delsing, and G. Johansson, "Designing frequency-dependent relaxation rates and Lamb shifts for a giant artificial atom", Physical Review A **90**, 013837 (2014).

[12] B. Kannan, M. J. Ruckriegel, D. L. Campbell, A. Frisk Kockum, J. Braumüller, D. K. Kim, M. Kjaergaard, P. Krantz, A. Melville, B. M. Niedzielski, A. Vepsäläinen, R. Winik, J. L. Yoder, F. Nori, T. P. Orlando, S. Gustavsson, and W. D. Oliver, "Waveguide quantum electrodynamics with superconducting artificial giant atoms", Nature **583**, 775–779 (2020).

[13] T. Aref, P. Delsing, M. K. Ekström, A. F. Kockum, M. V. Gustafsson, G. Johansson, P. J. Leek, E. Magnusson, and R. Manenti, in *Superconducting Devices in Quantum Optics*, edited by R. H. Hadfield and G. Johansson (Springer, 2016).

[14] R. Manenti, A. F. Kockum, A. Patterson, T. Behrle, J. Rahamim, G. Tancredi, F. Nori, and P. J. Leek, "Circuit quantum acoustodynamics with surface acoustic waves", Nature Communications **8**, 975 (2017).

[15] A. Noguchi, R. Yamazaki, Y. Tabuchi, and Y. Nakamura, "Qubit-Assisted Transduction for a Detection of Surface Acoustic Waves near the Quantum Limit", Physical Review Letters **119**, 180505 (2017).

[16] K. J. Satzinger, Y. P. Zhong, H.-S. Chang, G. A. Peairs, A. Bienfait, M.-H. Chou, A. Y. Cleland, C. R. Conner, É. Dumur, J. Grebel, I. Gutierrez, B. H. November, R. G. Povey, S. J. Whiteley, D. D. Awschalom, D. I. Schuster, and A. N. Cleland, "Quantum control of surface acoustic-wave phonons", Nature **563**, 661 (2018).

[17] B. A. Moores, L. R. Sletten, J. J. Viennot, and K. W. Lehnert, "Cavity Quantum Acoustic Device in the Multimode Strong Coupling Regime", Physical Review Letters **120**, 227701 (2018).

[18] A. N. Bolgar, J. I. Zotova, D. D. Kirichenko, I. S. Besedin, A. V. Semenov, R. S. Shaikhaidarov, and O. V. Astafiev, "Quantum Regime of a Two-Dimensional Phonon Cavity", Physical Review Letters **120**, 223603 (2018).

[19] L. R. Sletten, B. A. Moores, J. J. Viennot, and K. W. Lehnert, "Resolving Phonon Fock States in a Multimode Cavity with a Double-Slit Qubit", Physical Review X **9**, 021056 (2019).

[20] A. Bienfait, K. J. Satzinger, Y. P. Zhong, H.-S. Chang, M.-H. Chou, C. R. Conner, É. Dumur, J. Grebel, G. A. Peairs, R. G. Povey, and A. N. Cleland, "Phonon-mediated quantum state transfer and remote qubit entanglement", Science **364**, 368 (2019).

[21] G. Andersson, B. Suri, L. Guo, T. Aref, and P. Delsing, "Non-exponential decay of a giant artificial atom", Nature Physics **15**, 1123–1127 (2019).

[22] A. Bienfait, Y. P. Zhong, H.-S. Chang, M.-H. Chou, C. R. Conner, É. Dumur, J. Grebel, G. A. Peairs, R. G. Povey, K. J. Satzinger, and A. N. Cleland, "Quantum Erasure Using Entangled Surface Acoustic Phonons", Physical Review X **10**, 021055 (2020).

[23] G. Andersson, M. K. Ekström, and P. Delsing, "Electromagnetically Induced Acoustic Transparency with a Superconducting Circuit", Physical Review Letters **124**, 240402 (2020).

[24] A. M. Vadiraj, A. Ask, T. G. McConkey, I. Nsanzineza, C. W. S. Chang, A. F. Kockum, and C. M. Wilson, "Engineering the level structure of a giant artificial atom in waveguide quantum electrodynamics", Physical Review A **103**, 023710 (2021).

[25] A. González-Tudela, C. S. Muñoz, and J. I. Cirac, "Engineering and Harnessing Giant Atoms in High-Dimensional Baths: A Proposal for Implementation with Cold Atoms", Physical Review Letters **122**, 203603 (2019).

[26] L. Du, Y. Zhang, J. H. Wu, A. F. Kockum, and Y. Li, "Giant Atoms in a Synthetic Frequency Dimension", Physical Review Letters **128**, 223602 (2022).

[27] P. O. Guimond, B. Vermersch, M. L. Juan, A. Sharafiev, G. Kirchmair, and P. Zoller, "A unidirectional on-chip photonic interface for superconducting circuits", npj Quantum Information **6** (2020).

[28] N. Gheeraert, S. Kono, and Y. Nakamura, "Programmable directional emitter and receiver of itinerant microwave photons in a waveguide", Physical Review A **102**, 053720 (2020).

[29] Y. X. Zhang, C. R. I Carceller, M. Kjaergaard, and A. S. Sørensen, "Charge-Noise Insensitive Chiral Photonic Interface for Waveguide Circuit QED", Physical Review Letters **127**, 233601 (2021).

[30] B. Kannan, A. Almanakly, Y. Sung, A. Di Paolo, D. A. Rower, J. Braumüller, A. Melville, B. M. Niedzielski, A. Karamlou, K. Serniak, A. Vepsäläinen, M. E. Schwartz, J. L. Yoder, R. Winik, J. I. Wang, T. P. Orlando, S. Gustavsson, J. A. Grover, and W. D. Oliver, "On-demand directional microwave photon emission using waveguide quantum electrodynamics", Nature Physics (2023).

[31] Z. Q. Wang, Y. P. Wang, J. Yao, R. C. Shen, W. J. Wu, J. Qian, J. Li, S. Y. Zhu, and J. Q. You, "Giant spin ensembles in waveguide magnonics", Nature communications **13**, 7580 (2022).

[32] A. J. Daley, I. Bloch, C. Kokail, S. Flannigan, N. Pearson, M. Troyer, and P. Zoller, "Practical quantum advantage in quantum simulation", Nature **607**, 667–676 (2022).

[33] A. Frisk Kockum, G. Johansson, and F. Nori, "Decoherence-Free Interaction between Giant Atoms in Waveguide Quantum Electrodynamics", Physical Review Letters **120**, 140404 (2018).

[34] A. Carollo, D. Cilluffo, and F. Ciccarello, "Mechanism of decoherence-free coupling between giant atoms", Physical Review Research **2**, 043184 (2020).

[35] L. Guo, A. F. Kockum, F. Marquardt, and G. Johansson, "Oscillating bound states for a giant atom", Physical Review Research **2**, 043014 (2020).

[36] J. T. Shen and S. Fan, "Coherent photon transport from spontaneous emission in one-dimensional waveguides", Optics Letters **30**, 2001–2003 (2005).

[37] J. T. Shen and S. Fan, "Coherent Single Photon Transport in a One-Dimensional Waveguide Coupled with Superconducting Quantum Bits", Physical Review Letters **95**, 213001 (2005).

[38] I. De Vega and D. Alonso, "Dynamics of non-Markovian open quantum systems", Reviews of Modern Physics **89**, 015001 (2017).

[39] D. Roy, C. M. Wilson, and O. Firstenberg, "Colloquium: Strongly interacting photons in one-dimensional continuum", Reviews of Modern Physics **89**, 021001 (2017).

[40] H. J. Carmichael, *Statistical Methods in Quantum Optics 1* (Springer-Verlag Berlin Heidelberg, 1999).

[41] J. Gough and M. R. James, "Quantum Feedback Networks: Hamiltonian Formulation", Communications in Mathematical Physics **287**, 1109–1132 (2009).

[42] J. Gough and M. R. James, "The Series Product and Its Application to Quantum Feedforward and Feedback Networks", IEEE Transactions on Automatic Control **54**, 2530–2544 (2009).

[43] J. Combes, J. Kerckhoff, and M. Sarovar, "The SLH framework for modeling quantum input-output networks", Advances in Physics: X **2**, 784–888 (2017).

[44] A. Frisk Kockum, *Quantum Optics with Semiconducting Artificial Atoms*, Ph.D. thesis, Chalmers University of Technology (2014).

[45] F. Bloch and A. Siegert, "Magnetic Resonance for Nonrotating Fields", Physical Review **57**, 522 (1940).

[46] G. S. Agarwal, "Rotating-Wave Approximation and Spontaneous Emission", Physical Review A **7**, 1195 (1973).

[47] G. S. Agarwal, "Quantum statistical theories of spontaneous emission and their relation to other approaches", in *Quantum Optics*, edited by G. Höhler (Springer Berlin Heidelberg, Berlin, Heidelberg, 1974) pp. 1–128.

[48] C. W. Gardiner, "Driving a quantum system with the output field from another driven quantum system", Physical Review Letters **70**, 2269 (1993).

[49] H. J. Carmichael, "Quantum trajectory theory for cascaded open systems", Physical Review Letters **70**, 2273 (1993).

[50] J. Kerckhoff, *Quantum Engineering with Quantum Optics*, Ph.D. thesis, Standford University (2011).

[51] R. Mitsch, C. Sayrin, B. Albrecht, P. Schneeweiss, and A. Rauschenbeutel, "Quantum state-controlled directional spontaneous emission of photons into a nanophotonic waveguide", Nature Communications **5**, 5713 (2014).

[52] J. Petersen, J. Volz, and A. Rauschenbeutel, "Chiral nanophotonic waveguide interface based on spin-orbit interaction of light", Science **346**, 67–71 (2014).

[53] K. Y. Bliokh and F. Nori, "Transverse and longitudinal angular momenta of light", Physics Reports **592**, 1–38 (2015).

[54] S. J. Masson and A. Asenjo-Garcia, "Atomic-waveguide quantum electrodynamics", Physical Review Research **2**, 043213 (2020).

[55] X. Gu, A. F. Kockum, A. Miranowicz, Y.-X. Liu, and F. Nori, "Microwave photonics with superconducting quantum circuits", Physics Reports **718-719**, 1–102 (2017).

[56] S. R. Sathyamoorthy, L. Tornberg, A. F. Kockum, B. Q. Baragiola, J. Combes, C. M. Wilson, T. M. Stace, and G. Johansson, "Quantum Nondemolition Detection of a Propagating Microwave Photon", Physical Review Letters **112**, 093601 (2014).

[57] K. M. Sliwa, M. Hatridge, A. Narla, S. Shankar, L. Frunzio, R. J. Schoelkopf, and M. H. Devoret, "Reconfigurable Josephson Circulator/Directional Amplifier", Physical Review X **5**, 041020 (2015).

[58] B. J. Chapman, E. I. Rosenthal, J. Kerckhoff, B. A. Moores, L. R. Vale, J. A. B. Mates, G. C. Hilton, K. Lalumière, A. Blais, and K. W. Lehnert, "Widely Tunable On-Chip Microwave Circulator for Superconducting Quantum Circuits", Physical Review X **7**, 041043 (2017).

[59] C. Müller, S. Guan, N. Vogt, J. H. Cole, and T. M. Stace, "Passive On-Chip Superconducting Circulator Using a Ring of Tunnel Junctions", Physical Review Letters **120**, 213602 (2018).

[60] E. Sánchez-Burillo, C. Wan, D. Zueco, and A. González-Tudela, "Chiral quantum optics in photonic sawtooth lattices", Physical Review Research **2**, 023003 (2020).

[61] Y.-J. Lin, K. Jiménez-García, and I. B. Spielman, "Spin–orbit-coupled Bose–Einstein condensates", Nature **471**, 83–86 (2011).

[62] V. Galitski and I. B. Spielman, "Spin–orbit coupling in quantum gases", Nature **494**, 49–54 (2013).

[63] T. Ramos, H. Pichler, A. J. Daley, and P. Zoller, "Quantum Spin Dimers from Chiral Dissipation in Cold-Atom Chains", Physical Review Letters **113**, 237203 (2014).

[64] B. Vermersch, T. Ramos, P. Hauke, and P. Zoller, "Implementation of chiral quantum optics with Rydberg and trapped-ion setups", Physical Review A **93**, 063830 (2016).

[65] A. F. van Loo, R. G. E. Morris, and A. D. Karenowska, "Time-Resolved Measurements of Surface Spin-Wave Pulses at Millikelvin Temperatures", Physical Review Applied **10**, 044070 (2018).

[66] T. Ramos, B. Vermersch, P. Hauke, H. Pichler, and P. Zoller, "Non-Markovian dynamics in chiral quantum networks with spins and photons", Physical Review A **93**, 062104 (2016).

[67] K. Stannigel, P. Rabl, and P. Zoller, "Driven-dissipative preparation of entangled states in cascaded quantum-optical networks", New Journal of Physics **14**, 063014 (2012).

[68] C. Gonzalez-Ballestero, A. Gonzalez-Tudela, F. J. Garcia-Vidal, and E. Moreno, "Chiral route to spontaneous entanglement generation", Physical Review B **92**, 155304 (2015).

[69] H. Pichler, T. Ramos, A. J. Daley, and P. Zoller, "Quantum optics of chiral spin networks", Physical Review A **91**, 42116 (2015).

[70] P.-O. Guimond, H. Pichler, A. Rauschenbeutel, and P. Zoller, "Chiral quantum optics with V-level atoms and coherent quantum feedback", Physical Review A **94**, 033829 (2016).

[71] P. Lodahl, S. Mahmoodian, S. Stobbe, A. Rauschenbeutel, P. Schneeweiss, J. Volz, H. Pichler, and P. Zoller, "Chiral quantum optics", Nature **541**, 473–480 (2017).

[72] M. Bello, G. Platero, J. I. Cirac, and A. González-Tudela, "Unconventional quantum optics in topological waveguide QED", Science Advances **5**, eaaw0297 (2019).

[73] T. Ozawa, H. M. Price, A. Amo, N. Goldman, M. Hafezi, L. Lu, M. C. Rechtsman, D. Schuster, J. Simon, O. Zilberberg, and I. Carusotto, "Topological photonics", Reviews of Modern Physics **91**, 015006 (2019).

[74] M. Scheucher, J. Volz, and A. Rauschenbeutel, in *Ultra-High-Q Optical Microcavities*, edited by Y.-F. Xiao, C.-L. Zou, Q. Gong, and L. Yang (World Scientific, 2020) Chap. 5, pp. 159–201.

[75] S. Mahmoodian, G. Calajó, D. E. Chang, K. Hammerer, and A. S. Sørensen, "Dynamics of Many-Body Photon Bound States in Chiral Waveguide QED", Physical Review X **10**, 031011 (2020).

[76] E. Kim, X. Zhang, V. S. Ferreira, J. Banker, J. K. Iverson, A. Sipahigil, M. Bello, A. González-Tudela, M. Mirhosseini, and O. Painter, "Quantum Electrodynamics in a Topological Waveguide", Physical Review X **11**, 011015 (2021).

[77] R. H. Dicke, "Coherence in Spontaneous Radiation Processes", Physical Review **93**, 99 (1954).

[78] R. H. Lehmberg, "Radiation from an N-Atom System. II. Spontaneous Emission from a Pair of Atoms", Physical Review A **2**, 889 (1970).

[79] G. Lenz and P. Meystre, "Resonance fluorescence from two identical atoms in a standing-wave field", Phys. Rev. A **48**, 3365 (1993).

[80] F. Le Kien, S. D. Gupta, K. P. Nayak, and K. Hakuta, "Nanofiber-mediated radiative transfer between two distant atoms", Physical Review A **72**, 063815 (2005).

[81] K. Lalumière, B. C. Sanders, A. F. van Loo, A. Fedorov, A. Wallraff, and A. Blais, "Input-output theory for waveguide QED with an ensemble of inhomogeneous atoms", Physical Review A **88**, 043806 (2013).

[82] M. Fleischhauer and M. D. Lukin, "Quantum memory for photons: Dark-state polaritons", Physical Review A **65**, 022314 (2002).

[83] A. I. Lvovsky, B. C. Sanders, and W. Tittel, "Optical quantum memory", Nature Photonics **3**, 706–714 (2009).

[84] K. Heshami, D. G. England, P. C. Humphreys, P. J. Bustard, V. M. Acosta, J. Nunn, and B. J. Sussman, "Quantum memories: emerging applications and recent advances", Journal of Modern Optics **63**, 2005–2028 (2016).

[85] H. J. Kimble, "The quantum internet", Nature **453**, 1023–1030 (2008).

[86] S. Wehner, D. Elkouss, and R. Hanson, "Quantum internet: A vision for the road ahead", Science **362**, eaam9288 (2018).

[87] G. Calajó, F. Ciccarello, D. Chang, and P. Rabl, "Atom-field dressed states in slow-light waveguide QED", Physical Review A **93**, 033833 (2016).

[88] I. Carusotto, A. A. Houck, A. J. Kollár, P. Roushan, D. I. Schuster, and J. Simon, "Photonic materials in circuit quantum electrodynamics", Nature Physics **16**, 268–279 (2020).

[89] J. D. Hood, A. Goban, A. Asenjo-Garcia, M. Lu, S. P. Yu, D. E. Chang, and H. J. Kimble, "Atom-atom interactions around the band edge of a photonic crystal waveguide", Proceedings of the National Academy of Sciences of the United States of America **113**, 10507–10512 (2016).

[90] L. Krinner, M. Stewart, A. Pazmiño, J. Kwon, and D. Schneble, "Spontaneous emission of matter waves from a tunable open quantum system", Nature **559**, 589–592 (2018).

[91] M. Stewart, J. Kwon, A. Lanuza, and D. Schneble, "Dynamics of matter-wave quantum emitters in a structured vacuum", Physical Review Research **2**, 043307 (2020).

[92] Y. Liu and A. A. Houck, "Quantum electrodynamics near a photonic bandgap", Nature Physics **13**, 48–52 (2017).

[93] N. M. Sundaresan, R. Lundgren, G. Zhu, A. V. Gorshkov, and A. A. Houck, "Interacting Qubit-Photon Bound States with Superconducting Circuits", Physical Review X **9**, 011021 (2019).

[94] P. M. Harrington, M. Naghiloo, D. Tan, and K. W. Murch, "Bath engineering of a fluorescing artificial atom with a photonic crystal", Physical Review A **99**, 052126 (2019).

[95] M. Mirhosseini, E. Kim, V. S. Ferreira, M. Kalaee, A. Sipahigil, A. J. Keller, and O. Painter, "Superconducting metamaterials for waveguide quantum electrodynamics", Nature Communications **9**, 3706 (2018).

[96] S. Indrajeet, H. Wang, M. D. Hutchings, B. G. Taketani, F. K. Wilhelm, M. D. Lahaye, and B. L. Plourde, "Coupling a Superconducting Qubit to a Left-Handed Metamaterial Resonator", Physical Review Applied **14**, 064033 (2020).

[97] V. S. Ferreira, J. Banker, A. Sipahigil, M. H. Matheny, A. J. Keller, E. Kim, M. Mirhosseini, and O. Painter, "Collapse and Revival of an Artificial Atom Coupled to a Structured Photonic Reservoir", Physical Review X **11**, 41043 (2021).

[98] M. Scigliuzzo, G. Calajò, F. Ciccarello, D. Perez Lozano, A. Bengtsson, P. Scarlino, A. Wallraff, D. Chang, P. Delsing, and S. Gasparinetti, "Controlling Atom-Photon Bound States in an Array of Josephson-Junction Resonators", Physical Review X **12**, 31036 (2022).

[99] J. S. Douglas, H. Habibian, C. L. Hung, A. V. Gorshkov, H. J. Kimble, and D. E. Chang, "Quantum many-body models with cold atoms coupled to photonic crystals", Nature Photonics **9**, 326–331 (2015).

[100] A. González-Tudela, C. L. Hung, D. E. Chang, J. I. Cirac, and H. J. Kimble, "Subwavelength vacuum lattices and atom-atom interactions in two-dimensional photonic crystals", Nature Photonics **9**, 320–325 (2015).

[101] D. E. Chang, J. S. Douglas, A. González-Tudela, C. L. Hung, and H. J. Kimble, "Colloquium: Quantum matter built from nanoscopic lattices of atoms and photons", Reviews of Modern Physics **90**, 31002 (2018).

[102] V. P. Bykov, "Spontaneous Emission From a Medium With a Band Spectrum.", Soviet Journal of Quantum Electronics **4**, 861 (1975).

[103] S. John and T. Quang, "Spontaneous emission near the edge of a photonic band gap", Physical Review A **50**, 1764 (1994).

[104] A. G. Kofman, G. Kurizki, and B. Sherman, "Spontaneous and induced atomic decay in photonic band structures", Journal of Modern Optics **41**, 353–384 (1994).

[105] S. Bay, P. Lambropoulos, and K. Mølmer, "Atom-atom interaction in strongly modified reservoirs", Physical Review A **55**, 1485 (1997).

[106] P. Lambropoulos, G. M. Nikolopoulos, T. R. Nielsen, and S. Bay, "Fundamental quantum optics in structured reservoirs", Reports on Progress in Physics **63**, 455 (2000).

[107] E. Shahmoon and G. Kurizki, "Nonradiative interaction and entanglement between distant atoms", Physical Review A **87**, 033831 (2013).

[108] X. Zhang, E. Kim, D. K. Mark, S. Choi, and O. Painter, "A superconducting quantum simulator based on a photonic-bandgap metamaterial", Science **379**, 278–283 (2023).

[109] C. Tabares, A. M. de las Heras, L. Tagliacozzo, D. Porras, and A. González-Tudela, "Variational waveguide QED simulators", arXiv:2302.01922 [quant-ph] (2023).

[110] A. González-Tudela and J. I. Cirac, "Markovian and non-Markovian dynamics of quantum emitters coupled to two-dimensional structured reservoirs", Physical Review A **96**, 043811 (2017).

[111] C. Cohen-Tannoudji, J. Dupont-Roc, and G. Grynberg, "Nonperturbative Calculation of Transition Amplitudes", in *Atom—Photon Interactions* (John Wiley & Sons, Ltd, 1998) Chap. 3, pp. 165–255.

[112] E. T. Whittaker and G. N. Watson, *A Course of Modern Analysis* (Cambridge University Press, 1996).

[113] X. Wang and H.-r. Li, "Chiral quantum network with giant atoms", Quantum Science and Technology **7**, 035007 (2022).

[114] M. Baur, S. Filipp, R. Bianchetti, J. M. Fink, M. Göppl, L. Steffen, P. J. Leek, A. Blais, and A. Wallraff, "Measurement of Autler-Townes and Mollow Transitions in a Strongly Driven Superconducting Qubit", Physical Review Letters **102**, 243602 (2009).

[115] L. Du, Y.-T. Chen, and Y. Li, "Nonreciprocal frequency conversion with chiral Λ-type atoms", Physical Review Research **3**, 043226 (2021).

[116] K. Bergmann, H. Theuer, and B. W. Shore, "Coherent population transfer among quantum states of atoms and molecules", Reviews of Modern Physics **70**, 1003 (1998).

[117] K. Bergmann, N. V. Vitanov, and B. W. Shore, "Perspective: Stimulated Raman adiabatic passage: The status after 25 years", The Journal of Chemical Physics **142**, 170901 (2015).

[118] N. V. Vitanov, A. A. Rangelov, B. W. Shore, and K. Bergmann, "Stimulated Raman adiabatic passage in physics, chemistry, and beyond", Reviews of Modern Physics **89**, 015006 (2017).

[119] S. J. Masson and A. Asenjo-Garcia, "Universality of Dicke superradiance in arrays of quantum emitters", Nature Communications **13**, 2285 (2022).

[120] C. Liedl, F. Tebbenjohanns, C. Bach, A. Rauschenbeutel, and P. Schneeweiss, "Observation of superradiant bursts in waveguide QED", arXiv:2211.08940 [quant-ph] (2022).

[121] A. Albrecht, L. Henriet, A. Asenjo-Garcia, P. B. Dieterle, O. Painter, and D. E. Chang, "Subradiant states of quantum bits coupled to a one-dimensional waveguide", New Journal of Physics **21**, 025003 (2019).

[122] C. Vega, D. Porras, and A. González-Tudela, "Topological multi-mode waveguide QED", arXiv:2207.02090 [quant-ph] (2022).

[123] F. Schäfer, T. Fukuhara, S. Sugawa, Y. Takasu, and Y. Takahashi, "Tools for quantum simulation with ultracold atoms in optical lattices", Nature Reviews Physics **2**, 411–425 (2020).

[124] W. P. Su, J. R. Schrieffer, and A. J. Heeger, "Solitons in Polyacetylene", Physical Review Letters **42**, 1698 (1979).

[125] X. Wang, T. Liu, A. F. Kockum, H.-R. Li, and F. Nori, "Tunable Chiral Bound States with Giant Atoms", Physical Review Letters **126**, 43602 (2021).

[126] C. Vega, M. Bello, D. Porras, and A. González-Tudela, "Qubit-photon bound states in topological waveguides with long-range hoppings", Physical Review A **104**, 053522 (2021).

[127] W. Cheng, Z. Wang, and Y.-x. Liu, "Topology and retardation effect of a giant atom in a topological waveguide", Phys. Rev. A **106**, 033522 (2022).

[128] I. S. Besedin, M. A. Gorlach, N. N. Abramov, I. Tsitsilin, I. N. Moskalenko, A. A. Dobronosova, D. O. Moskalev, A. R. Matanin, N. S. Smirnov, I. A. Rodionov, A. N. Poddubny, and A. V. Ustinov, "Topological excitations and bound photon pairs in a superconducting quantum metamaterial", Physical Review B **103**, 224520 (2021).

[129] P. Roushan, C. Neill, A. Megrant, Y. Chen, R. Babbush, R. Barends, B. Campbell, Z. Chen, B. Chiaro, A. Dunsworth, A. Fowler, E. Jeffrey, J. Kelly, E. Lucero, J. Mutus, P. J. O'Malley, M. Neeley, C. Quintana, D. Sank, A. Vainsencher, J. Wenner, T. White, E. Kapit, H. Neven, and J. Martinis, "Chiral ground-state currents of interacting photons in a synthetic magnetic field", Nature Physics **13**, 146–151 (2017).

[130] C. Joshi, F. Yang, and M. Mirhosseini, "Resonance fluorescence of a chiral artificial atom", arXiv:2212.11400 [quant-ph] (2022).